

8-16-2024

Field Implementation of a Stereo Vision System for RNT and Stress Measurements in CWR

Brittany Stinson
University of South Carolina

Follow this and additional works at: <https://scholarcommons.sc.edu/etd>



Part of the [Civil Engineering Commons](#)

Recommended Citation

Stinson, B.(2024). *Field Implementation of a Stereo Vision System for RNT and Stress Measurements in CWR*. (Master's thesis). Retrieved from <https://scholarcommons.sc.edu/etd/7678>

This Open Access Thesis is brought to you by Scholar Commons. It has been accepted for inclusion in Theses and Dissertations by an authorized administrator of Scholar Commons. For more information, please contact digres@mailbox.sc.edu.

FIELD IMPLEMENTATION OF A STEREO VISION SYSTEM FOR RNT AND STRESS
MEASUREMENTS IN CWR

by

Brittany Nicole Stinson

Bachelor of Science
University of South Carolina, 2021

Submitted in Partial Fulfillment of the Requirements

For the Degree of Master of Science in

Civil Engineering

College of Engineering and Computing

University of South Carolina

2024

Accepted by:

Dimitris Rizos, Director of Thesis

Yu Qian, Reader

Robert Mullen, Reader

Ann Vail, Dean of the Graduate School

© Copyright by Brittany Nicole Stinson, 2024
All Rights Reserved

Dedication

This thesis is dedicated to my parents Patrick and Amy, my sister Katelyn, my grandfather “Pa,” my grandmother “Gramie” who passed before the completion of this work, and my closest friends, for without their unconditional support throughout this journey, I would not have been able to push myself to achieve what I hoped in life so far. I hope to have made them proud.

Acknowledgements

I would like to express my gratitude and thanks to the following people. First, thank you to my advisor Dr. Rizos for providing me the opportunity to further my education with a M.S. degree, and for the opportunity to work on this research project. With his continued support and encouragement, I have been able to grow as a person in my professional and personal life. I would also like to thank Dr. Mullen and Dr. Qian for being a part of my thesis committee and for their time and support throughout the project. Also, thank you to the undergraduate and other graduate students that provided help during laboratory and field testing, without their help this work would not have been possible.

This work has been partially funded by the Federal Railroad Administration (FRA) under contract 693JJ619C000007. The opinions expressed in this article are solely those of the authors and do not represent the opinions of the funding agency.

Abstract

The use of Continuous Welded Rail (CWR) provides many advantages to the rail industry compared to the alternatively used jointed-track segments. However, one significant disadvantage is the development of thermal stresses longitudinally in the rail, which is not of concern when expansion joints are used. This is due to CWR's inability to release thermal expansion in the absence of joints. The Rail Neutral Temperature (RNT) is the temperature at which the rail is in a stress-free state. A desired RNT is calculated based on local climate conditions and CWR installation practices are implemented to set the desired RNT at installation. Deviation of the RNT over time, along with temperature fluctuations and other contributing factors results in the development of longitudinal stresses and can cause track buckling or pull-apart, both of which pose significant risks regarding track safety and operations. Determining the RNT and the longitudinal stress in rail is important in effective rail stress management and preventing failures. Current methods used to determine the RNT in an existing track segment in service at any given time have many shortcomings, including the disruption of service, destruction of rail, and need for reference data.

Table of Contents

Dedication	iii
Acknowledgements	iv
Abstract	v
Chapter 1 Introduction	1
1.1 Industry Background and Problem Statement.....	1
1.2 Objectives and Scope of Work	3
1.3 Organization of Thesis	4
Chapter 2 RNT & DIC Background	5
2.1 Rail Neutral Temperature Measurement Technologies	5
2.2 Digital Image Correlation (DIC).....	9
Chapter 3 RNT & Stress Measurement Concept.....	15
3.1 Concept Development.....	15
3.2 Implementation.....	18
Chapter 4 System Configuration, Setup, and Verification.....	20
4.1 Instrumentation.....	20
4.2 System Configuration.....	26
4.3 Verification.....	31

4.4	Acquisition Platforms.....	33
Chapter 5	Data Acquisition and Processing	35
5.1	General Setup Procedure	35
5.2	Testing Procedure and Image Acquisition.....	38
5.3	Data Processing	39
Chapter 6	Field Implementation & Parametric Studies.....	41
6.1	Test Site	41
6.2	RNT Test Objectives	41
Chapter 7	Critical Discussion	70
7.1	Test 9 (Segment E0).....	70
7.2	Acquisition Platforms.....	70
7.3	Heating.....	71
7.4	Image Quality	71
7.5	Noise and Quality Control.....	73
7.6	Web and Stress Measurements.....	73
Chapter 8	Conclusions.....	74
8.1	Conclusions	74
8.2	Future Work.....	75
References	76

List of Tables

Table 2.1: Methods for RNT and Longitudinal Stress Measurements.....	7
Table 6.1: Field Test Conditions.....	42

List of Figures

Figure 1.1: Typical buckled track.....	2
Figure 2.1: Suggested (a) minimum speckle size by pixels, (b) subset size, and (c) speckle density (Wyatt, 2023).....	13
Figure 3.1: Hypothesis of RNT measurement concept based on rail constraints (red arrows): (a) non-uniform thermal expansion of TOR (orange arrows), and (b) development of negligible strain in the longitudinal direction & significant strain in the vertical direction (Knopf K. , 2019).....	16
Figure 3.2: Temperature - Curvature Relationship from Measurements	17
Figure 3.3: Temperature – Transverse (Vertical) Strain Relationship from Measurements.....	18
Figure 4.1: Rail cart system	21
Figure 4.2: (a) GS-U3-89S6M-C Grasshopper cameras, and (b) TechSpec lenses	22
Figure 4.3: (a) GS3-U3-91S6M-C Grasshopper cameras, and (b) Tamron lenses	23
Figure 5.1: (a) TOR and (b) web painted white	37
Figure 5.2: (a) TOR and (b) web speckled.....	37
Figure 5.3: Location of cameras mounted to frame and rail cart (circled in red)	38
Figure 6.2: Test 1 Station 1 Web Results	45
Figure 6.3: Test 2 Station 2 TOR Results.....	47
Figure 6.4: Test 2 Station 2 Web Results	48

Figure 6.5: Test 3 TOR Results (a) all, and (b) Averaged Reduced Temperature - Curvature Results.....	51
Figure 6.6: Test 3 Web Results (a) all, and (b) Reduced Temperature - Strain Results	53
Figure 6.7: Test 4 TOR Results	56
Figure 6.8: Test 4 Web Results.....	57
Figure 6.9: Test 5 (Segment A0) TOR Results	59
Figure 6.10: Test 5 (Segment A0) Web Results	60
Figure 6.11: Test 6 (Segment B0) TOR Results.....	61
Figure 6.12: Test 6 (Segment B0) Web Results	62
Figure 6.13: Test 8 (Segment D0) TOR Results	64
Figure 6.14: Test 8 (Segment D0) Web Results	65
Figure 6.15: Test 9 (Segment E0) TOR Results	66
Figure 6.17: Test 10 (Segment F0) TOR Results	68
Figure 7.1: Web calibration score for field testing 04-20-2023	72
Figure 7.2: Web cameras field of view zoomed in to show quality of images of (a) camera 0 and (b) camera 1	72

List of Abbreviations

CWR.....	Continuous Welded Rail
DIC.....	Digital Image Correlation
RNT.....	Rail Neutral Temperature
TOR.....	Top of Rail
PE.....	Projection Error

Chapter 1 Introduction

1.1 Industry Background and Problem Statement

Railroads have been a major component to the United States and the world economy due to the many advantages moving goods and people by rail. Freight railroads support almost every industry and account for moving one third of the US exports by volume. In the last five years, privately-owned major Class 1 freight railroads have invested annually approximately \$20 billion, on average, building and maintaining the rail network (Association of American Railroads, 2022). Proper, effective, and efficient maintenance is critical to maintaining the infrastructure in a state of good repair and support a safe operational network.

In recent years, continuous welded rail (CWR) has become the industry standard in track construction replacing jointed track. CWR eliminates rail joints providing a smooth riding surface and alleviates many of the well-documented disadvantages caused by jointed rail segments (Rizos, et al., 2022), (Knopf K. , A Non-Contacting System for Rail Neutral Temperature and Stress Measurements, 2019), and (Chao, 2022). However, because of the lack of joints, longitudinal stresses develop in the rail from thermal expansion. One key element in CWR maintenance is management of thermal stress and understanding the role of rail neutral temperature (RNT) in the development of longitudinal thermal stress in the rail. RNT is defined as the temperature at which the rail

in a CWR track is stress-free. Rail is installed in CWR track at a desired RNT determined based on regional climate conditions including average ambient temperature and projections for the area. CWR installation practices are then used to set this desired RNT independent of the ambient temperature at the time of installation. Factors such as operating conditions, repair, maintenance, track shifting, and track deformations cause RNT to deviate from the desired values increasing the risk of track buckling or rail pull apart (Knopf K. , Rizos, Qian, & Sutton, On the Validation and Implementation of a Vision-Based Concept for Rail Neutral Temperature and Stress Measurements, 2022) and (Knopf K. , A Non-Contacting System for Rail Neutral Temperature and Stress Measurements, 2019). An example of a typical buckled track is shown in Figure 1.1. Therefore, it is important to be able to accurately and efficiently assess the neutral temperature throughout the life of the rail and reset RNT to the desired values for effective thermal stress management.



Figure 1.1: Typical buckled track

Current methods used to determine the RNT and the thermal induced stress are destructive and disruptive, can be difficult to implement, and are known for system complexity, practicality, reliability, cost, and instrumentation demands (Knopf K. , 2019), while most are verified only under controlled laboratory conditions. Rizos and Knopf et al (Knopf K. , Rizos, Qian, & Sutton, 2020), (Knopf K. , Rizos, Qian, & Sutton, 2021), and (Knopf K. , Rizos, Qian, & Sutton, 2022), introduced a novel non-destructive, non-contacting, reference-free process for measuring RNT that has been validated both through laboratory testing and field measurements and is shown to be an accurate way to determine the RNT and stress state of the rail at any given without the need for reference data. The method belongs to the broader family of deformation methods and uses of machine vision, thermal scanning, and 3D Digital Image Correlation (StereoDIC) to facilitate the collection and extraction of deformation data.

1.2 Objectives and Scope of Work

Following Knopf's development of a novel method for estimating the RNT and longitudinal (axial) stress in rail (Knopf K. , 2019), and Chao's development of the first-generation prototype laboratory system (Chao, 2022), this thesis presents the development of the next generation that address the limitations of previous developments. The objectives of this thesis include:

1. Investigate the speckle requirements of the StereoDIC technology and optimize the speckle pattern and application method for field implementation.

2. Investigate the heating requirements of the employed RNT measurement technology, optimize the induced heating methods and assess the performance of the natural heating approach.
3. Investigate an alternate approach of data processing that allows the next generation system to be implemented on a mobile platform.
4. Assess the performance of the next generation in the laboratory and the field.

1.3 Organization of Thesis

The organization of this thesis is as follows:

Chapter 1: Introduces the problem statement and sets the scope of work for this thesis.

Chapter 2: Presents the background and important topics related to RNT and DIC technology.

Chapter 3: Discusses the concept development of RNT and stress measurements.

Chapter 4: Discusses the components of the DIC camera system and other supporting instrumentation.

Chapter 5: Discusses procedures related to setting up the StereoDIC camera system and steps for RNT measurement acquisition.

Chapter 6: Discusses field tests performed in 2022 and 2023.

Chapter 7: Discusses heating, image quality, noise, and web measurements, and gives recommendations.

Chapter 8: Discusses conclusions and recommendations.

Chapter 2 RNT & DIC Background

This chapter presents a summary of existing technologies for estimating rail neutral temperature as reported in the literature and a brief introduction of the Stereo Digital Image Correlation (StereoDIC) technology adopted in this work as the data acquisition system.

2.1 Rail Neutral Temperature Measurement Technologies

This section presents a summary of methods reported in the literature related to rail neutral temperature (RNT) measurement technologies. An extensive account of current techniques is reported in (Knopf K. , 2019), (Knopf K. , Rizos, Qian, & Sutton, 2020), (Knopf K. , Rizos, Qian, & Sutton, 2021), (Knopf K. , Rizos, Qian, & Sutton, 2022), (Chao, 2022), (Rizos, et al., 2022), (Stinson, Penna, Gedney, Rizos, & Sutton, 2023).

2.1.1 Current Methods

There are many techniques currently for estimating RNT and longitudinal stress measurements. These methods can be classified based on the underlying principles as: (i) rail cutting, (ii) rail lifting, (iii) deformation measurements, (iv) ultrasonic, (v) x-ray, (vi) magnetic, (vii) vibration, (viii) electrical impedance (piezoelectric), (ix) mechanical, (x) chemical, (xi) highly nonlinear solitary waves, and (xii) photoluminescence. Techniques (i) - (viii) have been discussed in detail in Knopf's work (Knopf K. , 2019), and

techniques (ix) - (xi) have been discussed in Chao’s work (Chao, 2022). A general account of the methods has also been presented in (Enshaeian & Rizzo, 2021). Table 2.1 is an extension of Knopf and Chao’s work to include the most recent works as of 2022. The table lists the existing technologies, based on the basic principles, outlines the shortcomings of each group of methods, and lists representative publications reported in the literature. Investigation into the use of photoluminescence piezospectroscopy has been done in recent years, however the validation and feasibility of this method has yet to be more thoroughly tested (Yun, Lee, Park, & Jung, 2019) and (Enshaeian & Rizzo, 2021).

Table 2.1 Methods for RNT and Longitudinal Stress Measurements

Method	Basic Principles	Shortcomings
(i) Rail Cutting	Cut rail to release thermal deformations for direct measurement of rail deformations.	<ul style="list-style-type: none"> • Time consuming • Destructive • Disruptive to train operations
(ii) Rail Lifting	An unclipped rail segment is lifted a predetermined distance. Resistance correlates with rail force and RNT.	<ul style="list-style-type: none"> • Time consuming • Semi-destructive • Disruptive to train operations • Rail must be in tension
(iii) Deformation Measurements	Uses strain gage, fiberoptics, or extensometer data to measure rail thermal elongation to compute stress.	<ul style="list-style-type: none"> • Contacting • Instrumentation installation • Relies on changing dimension • Stress-free reference measurement
(iv) Ultrasonic	The velocity of propagating sound waves in a medium is correlated to the stress state in rail.	<ul style="list-style-type: none"> • Contacting • Stress-free reference measurement • Sensitive to material structure/defects

		<ul style="list-style-type: none"> Assumes acoustic properties and residual stresses are constant
(v) X-Ray	Distance between two atomic planes in a crystal is measured through x-ray diffraction and related to material stresses.	<ul style="list-style-type: none"> Measures the stresses in a small volume close to the surface Stress-free reference measurement Distance data of the atomic planes in various material at various stress states Requires clean rail surface High instrumentation demands
(vi) Magnetic	Electromagnetic and acoustic response signals produce a magnetic field. The permeability in the magnet field is correlated to the longitudinal stress.	<ul style="list-style-type: none"> Time consuming calibration procedure Reference material measurement Barkhausen noise distribution depends on microstructure condition of rail material Influenced by residual stress High instrumentation demands
(vii) Vibration	Exciting rail to obtain vibration mode characteristics change with axial force	<ul style="list-style-type: none"> Contacting Stress-free reference measurement Instrumentation installation High instrumentation demands Insufficient accuracy because mode characteristics also depend on track conditions
(viii) Electrical Impedance (Piezoelectric)	The PZT excites the rail to obtain an EMI response signal from the rail that indicates deformation.	<ul style="list-style-type: none"> Contacting Instrumentation installation Within experimental stages
(ix) Mechanical	Beam-Column bending theory assumes the rail can be schematized as a simply	<ul style="list-style-type: none"> Time consuming Only applicable for tangent track

	supported beam under concentrated loading to estimate longitudinal stress in the track.	<ul style="list-style-type: none"> • Rail must be in tension • High Cost
(x) Chemical	Vibrational spectroscopy technique that measures residual stress in aluminum oxides through exciting the higher energy state by absorption of photonic energy.	<ul style="list-style-type: none"> • Requires accurate measurements • Early development stages
(xi) Highly Nonlinear Solitary Waves	HNSWs are enabled by a transducer. The transducer consists of a chain of steel particles inside a tube and surmounted by an electromagnet that has a striker that generates a solitary wave pulse that propagates and is detected by the sensor beads or by a force sensor.	<ul style="list-style-type: none"> • Still in the early development stages
(xii) Photoluminescence Piezospectroscopy (PLPS)	A low-power laser is used to detect alpha-phase aluminum oxide in thermite welds of CWR by measuring wavelengths.	<ul style="list-style-type: none"> • Highly sensitive equipment required • Possible weld-specific calibration required for each measurement • Still in development stages

Some of the methods successfully implemented in regular maintenance operations include rail cutting and rail lifting, which are the two most commonly used techniques. Other relatively successful methods include deformation measurements, magnetic, and x-ray. Other methods are currently in experimental stages, including ultrasonic, vibration, piezoelectric, and piezospectroscopy. All of these methods suffer from a variety of shortcomings related to the disruption of regular rail operations, destructive to the rail, require contact to the rail, ineffective methodologies, limited accuracy, simplicity of the method, high instrumentation demands, and the need for reference measurements.

Rizos (US Patent No. PCT/US2019/026267, 2018) introduced a novel concept for measuring RNT that was first validated in the work of Knopf and Rizos (Knopf K. , Rizos, Qian, & Sutton, On the Validation and Implementation of a Vision-Based Concept for Rail Neutral Temperature and Stress Measurements, 2022), (Knopf K. , A Non-Contacting System for Rail Neutral Temperature and Stress Measurements, 2019), (Knopf K. , Rizos, Qian, & Sutton, A non-contacting system for rail neutral temperature and stress measurements: Concept development, 2021), and implemented in the field in Chao and Rizos (Rizos, et al., 2022), (Chao, 2022). This novel concept alleviated the shortcomings of reported methods. However, the current configuration of the acquisition system requires that the system remains undisturbed and that the speckle remains intact throughout the duration of the test. This requirement restricts the ability to resume data acquisition in the event of a train passing over the test segment. The work presented in this thesis introduces a modification to the acquisition platform and data processing procedure that alleviates these issues.

2.2 Digital Image Correlation (DIC)

This section presents important topics related to digital image correlation fundamentals, and important components related to the implementation of the practice in the field.

2.2.1 Background

The theory of digital image correlation (DIC) started in the 1960s but was more thoroughly studied and developed in the 1980s at the University of South Carolina Laboratories. The concept was first implemented for in-plane deformation measurements (two-dimensional), however due to the nature of engineering applications and deformations being typically in a three-dimensional space, the technology evolved (M. A.

Sutton F. M., 2017), (M. A. Sutton J. J., 2009), (M. A. Sutton J. H.-J., 2008), (Standardization, 2018), (W. H. Peters III, 1983), (M. A. Sutton W. J., 1983). Over the past four decades, 3D-DIC (StereoDIC) has become a mature technology with a broad range of applications, including use in academia, government laboratories, and industry (M. A. Sutton F. M., 2017). StereoDIC has become applicable and advantageous in many industries, such as automotive and aerospace, due to it being (i) a non-contacting system, (ii) able to capture full-field surface deformations, (iii) able to acquire highly accurate measurements in the presence of both large rotations and displacements, (iv) able to be utilized for both curved and flat surfaces, and (v) able to allow for a variable field of view with the utilization of different lenses (Knopf K. , A Non-Contacting System for Rail Neutral Temperature and Stress Measurements, 2019), (Chao, 2022), (M. A. Sutton F. M., 2017), (M. A. Sutton J. J., 2009), (A. Abdulqader, 2020). In a single data acquisition, the StereoDIC system can acquire full-field measurements of shape, curvature, deformation, and strain (Knopf K. , A Non-Contacting System for Rail Neutral Temperature and Stress Measurements, 2019). This technology is commonly found in the aerospace and automotive industries and has recently been successfully implemented in quality control of pre-stressed concrete and material testing (Knopf K. , Rizos, Qian, & Sutton, A non-contacting system for rail neutral temperature and stress measurements: Concept development, 2021), (Abdulqader, 2017), (A. A. Rashid, 2020). In addition, StereoDIC has also been implemented in various railway-related applications, such as load testing and damage detection, performance assessment of prestressed concrete ties, ballast and fastener systems, determining opening stresses for railway steel under low cycle fatigue,

and monitoring dynamic displacements (Chao, 2022), (Abdulqader, 2017), (A. Abdulqader, 2020), (C. A. Murray, 2015), (A. A. Rashid, 2020).

2.2.2 Basic Procedure

Digital image correlation works by tracking the movement of an applied speckle pattern, that covers the area of interest, on the surface of a given material. A pair of cameras are then used to obtain image sets of the applied speckle pattern at different times throughout the deformation process. One pair of images are selected and used as the baseline image set. All other image sets are then correlated with respect to the baseline set in order to determine the movement of each speckle throughout the deformation process. This results in a 3D model of the material's deformation process across time. The theoretical background of image correlation is presented in detail in (M. A. Sutton J. J., 2009), (M. A. Sutton W. J., 1983), (W. H. Peters III, 1983). Best practices for acquisition and processing procedures are found in (Standardization, 2018). The speckle pattern and lighting conditions are of specific interest in this work and is discussed in the next section.

2.2.3 Speckle Pattern

One fundamental assumption of DIC is that the motion and deformation of the pattern that is imaged accurately replicates the motion and deformation of the underlying test specimen (Standardization, 2018). Therefore, two critical factors when implementing DIC technology are the application of a high contrast speckle pattern that adheres firmly to the material surface, and sufficient lighting of the specimen during image acquisition. Ensuring that the system has an optimal speckle pattern is critical for obtaining high-quality images that will yield accurate measurements.

Speckle patterns need to be designed based on four important aspects, i.e., the size of the speckle in view of the pixel resolution, contrast (grey levels), speckle edge sharpness (contrast gradient), and speckle density (spatial distribution) (Reu, The Art and Application of DIC; All about speckles, 2015), (Reu, The Art and Application of DIC; All About Speckles: Contrast, 2015), (Reu, The Art and Application of DIC; All About Speckles: Edge Sharpness, 2015), (Reu, The Art and Application of DIC; All about speckles: Speckle Density, 2015), (Reu, The Art and Application of DIC; Points on Paint, 2015), (Reu, The Art and Application of DIC; Speckle Size Measurement, 2014), (Reu, The Art and Application of DIC; Speckles and their relationship to the digital camera, 2014), (S. Yaofeng, 2007). The ideal speckle pattern should be of high contrast, with sharp edges and a randomized pattern with approximately fifty percent density. The speckle size should be such that speckles appear on the digital image at least as 3×3 pixel² (Figure 2.1a). This, the physical size of the speckle depends on the camera lens-to-object distance and the camera sensor resolution (Wyatt, 2023). Once the speckle size is determined, the pattern density should ideally be such that the black and white areas are well balanced (50% black – 50% white). Furthermore, the distribution of the speckle should show appropriate randomness so that subsets in different regions of the image may be uniquely identified (Figure 2.1b) (Standardization, 2018). The subset size should be large enough to include a minimum of 3 speckles by 3 speckles (Figure 2.1b). Any smaller than this dimension may result in incorrect deformation measurements, whereas a subset that is too large results in fewer data points (Wyatt, 2023).

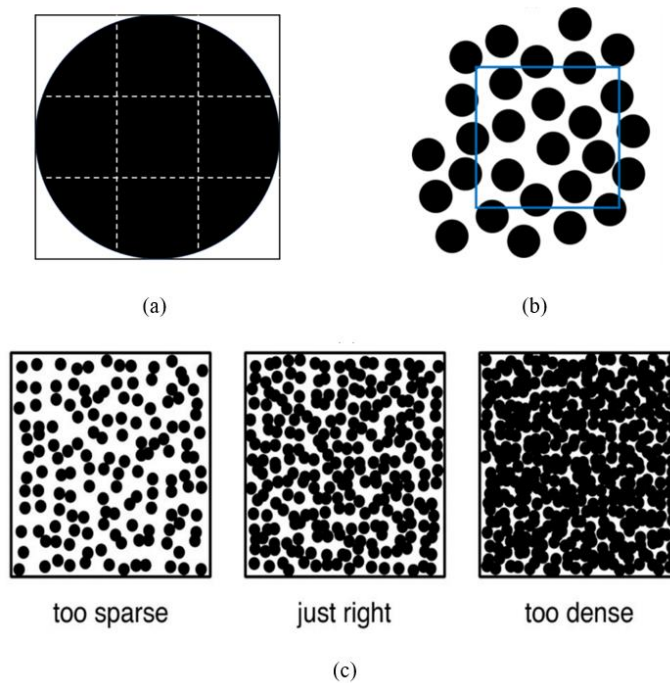


Figure 2.1: Suggested (a) minimum speckle size by pixels, (b) subset size, and (c) speckle density (Wyatt, 2023)

2.2.4 Lighting

Lighting is also an important aspect of DIC technology, as it helps to facilitate high contrast of the pattern on the specimen. Natural light is the easiest and preferred option, though it may not always be sufficient in practice. In this case, controlled lighting conditions may be used (Chao, 2022). A diffused light is recommended to avoid areas of high reflections and should be evenly distributed across the specimen. In order to reduce glare and reflections in the images, the pattern surface must have a matte, not glossy, finish (Standardization, 2018). When configuring the system for an experiment, there are several ways to adjust the lighting to remove or reduce reflections on the specimen surface. The artificial lighting can be physically moved closer or further away from the area of interest, or the intensity can be increased or decreased. The aperture of the

camera lenses should also be adjusted so that the resulting image is as bright as possible while also limiting reflections. Once the camera aperture is set, it cannot be adjusted after the system has been calibrated. Further adjustments to lighting after calibration should be to the physical lights and/or the shutter speed (in VIC-Snap) only. More detailed information regarding lighting and reflections can be found in (Standardization, 2018).

Chapter 3 RNT & Stress Measurement Concept

The chapter briefly discusses the method introduced by Rizos (US Patent No. PCT/US2019/026267, 2018) for measuring RNT and longitudinal stress and presented in detail in (Rizos, et al., 2022), (Knopf K. , Rizos, Qian, & Sutton, On the Validation and Implementation of a Vision-Based Concept for Rail Neutral Temperature and Stress Measurements, 2022), (Knopf K. , A Non-Contacting System for Rail Neutral Temperature and Stress Measurements, 2019), (Knopf K. , Rizos, Qian, & Sutton, A non-contacting system for rail neutral temperature and stress measurements: Concept development, 2021), (Knopf K. , Rizos, Qian, & Sutton, 2020), (Chao, 2022), (Stinson, Penna, Gedney, Rizos, & Sutton, 2023).

3.1 Concept Development

The development of the method used for determining the RNT of a given rail segment is based on two hypotheses: (a) Thermal loads will induce non-uniform deformations of the top of the rail in the transverse (vertical) direction, as depicted in Figure 3.1(a), due to the constraints imposed by the continuity of the rail in the longitudinal direction, and/or the anchoring of the rail to the ties; and (b) Under thermal loads, the web of the rail at a location between two consecutive ties remains nearly stress free in the transverse direction and, thus, the total transverse strain, ϵ_y , is dominated by the thermal strain component that directly depends on the temperature change. In contrast, the rail

constraints prevent thermal deformations in the longitudinal direction, inducing significant stress. Thus, the total longitudinal strain, ϵ_x , becomes negligible, since the constraints prevent any thermal strain, as depicted in Figure 3.1b. Both hypotheses have been validated in FEM simulations and laboratory testing as reported in (Rizos, et al., 2022), (Knopf K. , Rizos, Qian, & Sutton, On the Validation and Implementation of a Vision-Based Concept for Rail Neutral Temperature and Stress Measurements, 2022), (Knopf K. , A Non-Contacting System for Rail Neutral Temperature and Stress Measurements, 2019), (Knopf K. , Rizos, Qian, & Sutton, A non-contacting system for rail neutral temperature and stress measurements: Concept development, 2021), (Knopf K. , Rizos, Qian, & Sutton, 2020), (Chao, 2022), (Stinson, Penna, Gedney, Rizos, & Sutton, 2023).

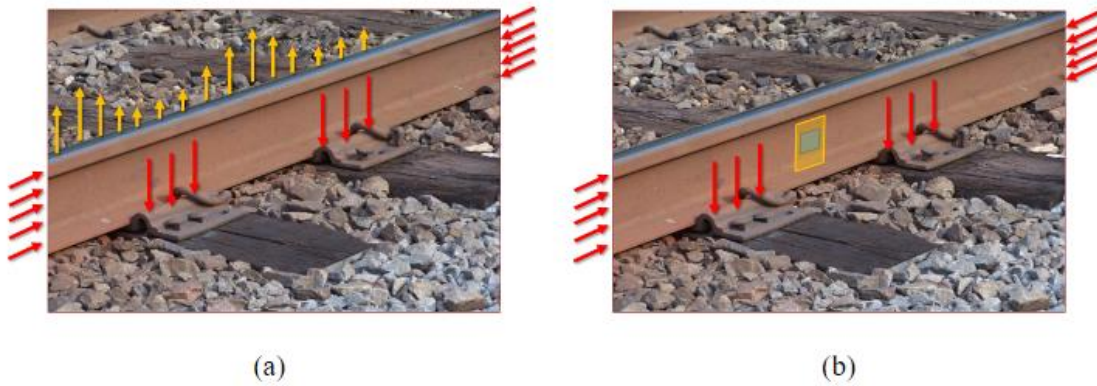


Figure 3.1: Hypothesis of RNT measurement concept based on rail constraints (red arrows): (a) non-uniform thermal expansion of TOR (orange arrows), and (b) development of negligible strain in the longitudinal direction & significant strain in the vertical direction (Knopf K. , 2019)

These studies demonstrated that the curvature along the length of the top of rail changes linearly as temperature changes. Furthermore, the sign of the curvature changes as the temperature traverses RNT. This indicates that RNT can be estimated in theory by measuring curvatures, k_1 and k_2 , along the top of rail at two distinct temperatures, T_1 and

T_2 . The pair of points (T_1, k_1) and (T_2, k_2) define the corresponding equation that expresses the linear temperature-curvature relationship, shown in Figure 3.2, the intercept of which is the sought after RNT defined as:

$$RNT = T_2 - k_2 \left[\frac{T_2 - T_1}{k_2 - k_1} \right] \quad (1)$$

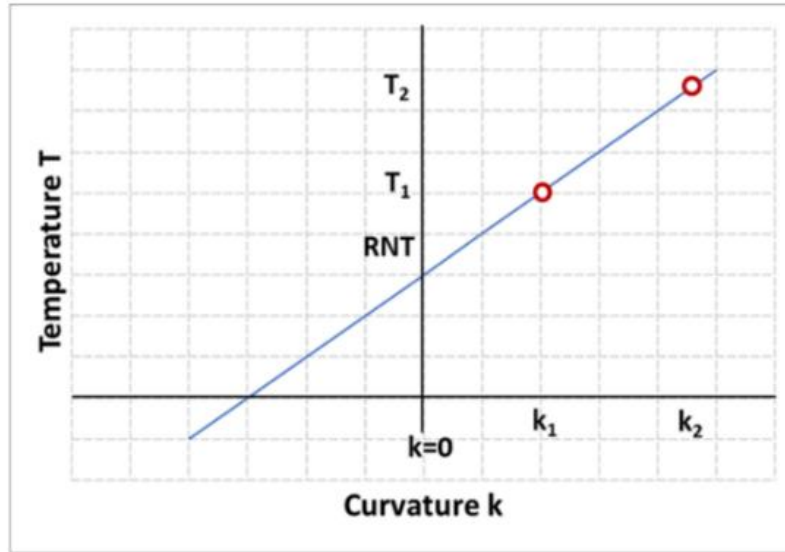


Figure 3.2: Temperature - Curvature Relationship from Measurements

The second hypothesis has also been validated and, furthermore, it is shown that:

- (a) stress is negligible in the transverse direction where maximum strain is observed;
- (b) stress is maximum in the longitudinal direction where negligible strain is observed, and
- (c) strain and stress change linearly as temperature changes.

This implies that, once the RNT is estimated as indicated in Equation (1), and strain change $(\Delta \epsilon_y)$ measurements at the web are taken for a corresponding temperature change (ΔT) , a unique temperature-strain relationship, shown in Figure 3.3, is defined as:

$$T = RNT + \left(\frac{\Delta T}{\Delta \epsilon_y}\right)\epsilon_y \quad (2)$$

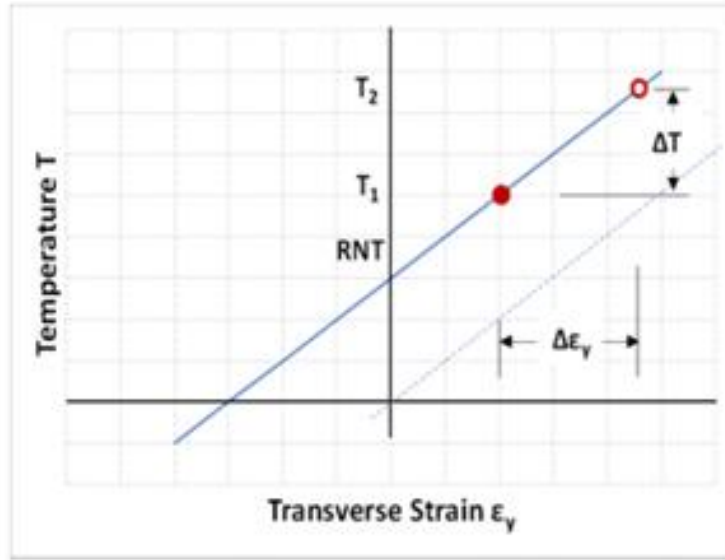


Figure 3.3: Temperature – Transverse (Vertical) Strain Relationship from Measurements

These studies conclude that the longitudinal stress at a given temperature can be determined as a function of the measured longitudinal and transverse strain in the web and the material properties of the rail. Assuming plane-stress conditions in the web with no initial strains at RNT and that the transverse stress, σ_y , is negligible, the sought after longitudinal stress is computed as:

$$\sigma_x \approx \frac{E}{(1+\nu)} (\epsilon_x - \epsilon_y) \quad (3)$$

3.2 Implementation

Digital Image Correlation technology is used to obtain the shape and deformation measurements needed to determine the RNT and stress in a rail segment. The rail is heated using either a natural or an induced heating cycle, and measurements can be taken without the need to bracket the RNT. Figure 3.4 below provides an example of successful

measurements taken in the field. It is critical that once the system is in place, the only changes should come from the heating of the rail. The cameras must remain in a fixed position, and the speckle pattern on the rail must remain intact throughout the duration of the test. Any change in these components disrupts the ability to accurately correlate any deformations across temperatures.

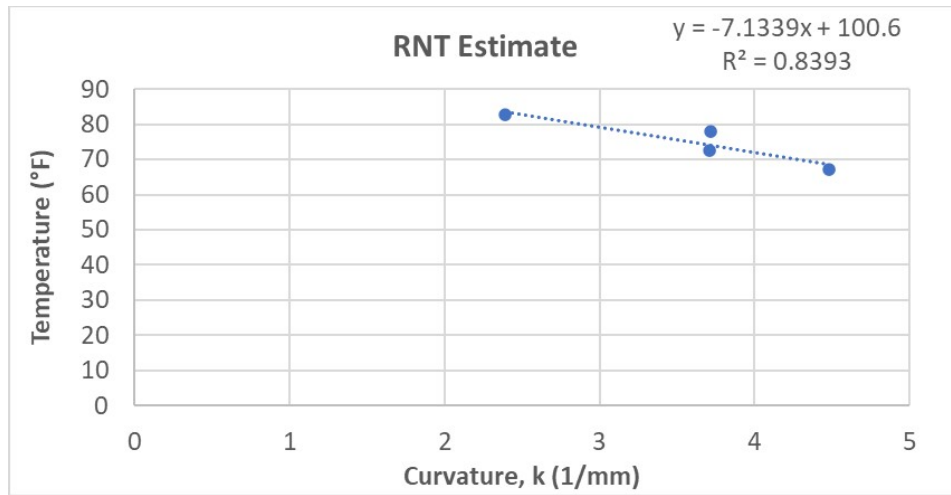


Figure 3.4: Example RNT Estimation

Chapter 4 System Configuration, Setup, and Verification

The deformation and strain measurements required in estimating the RNT through the proposed technique are acquired using StereoDIC technology. The first generation prototype was based on a stationary system, due to the limitations of the technology that required the Digital Image Correlation to be performed across temperatures. This work introduces an alternate way of processing the data, as discussed in the forthcoming section, that eliminates this limitation. The second generation of the system is launched from a moving platform. The primary components of the data acquisition system are common to both. This chapter introduces the second-generation prototype system and discusses the platform, its primary components, and other supporting instrumentation.

4.1 Instrumentation

The StereoDIC data acquisition system comprises two pairs of optical digital cameras, an infrared camera, lighting, and data acquisition hardware and software. The acquisition system is powered by a solar power generator and all components are mounted on a rail cart facilitating data acquisition at multiple locations from a moving platform, as shown in Figure 4.1. Supporting equipment includes speckling equipment, system calibration targets, and rail heaters powered by a stand along gasoline powered generator.



Figure 4.1: Rail cart system

4.1.1 StereoDIC Cameras

The top of rail StereoDIC system consists of a pair of GS3-U3-89S6M-C USB3.0 Grasshopper 8.9MP cameras, as shown in Figure 4.2(a). The cameras are based on a Sony IMX255 sensor, 1" format, with 3.45 μm pixel size. The acquisition rate is 43 frames per second at 4096 x 2160 pixel² resolution. The cameras are equipped with TechSpec High Resolution lenses with a 16mm focal length (Figure 4.2b). Blue filters are placed on the lenses to be used in conjunction with blue LED lights. The pair of cameras are semi-permanently mounted to an approximately 20-inch carbon fiber bar with four 8mm T-slots, shown in Figure 4.4. The carbon fiber bar was chosen due its very low coefficient of thermal expansion ensuring that the relative position of the cameras will not change when the assembly is exposed to temperature changes in the field. The camera assembly can be easily attached and detached through a fast release clip to the

articulated arm that is permanently fixed to the rail cart. This configuration facilitates the pre-calibration of the system and reduces the setup time.



Figure 4.2: (a) GS-U3-89S6M-C Grasshopper cameras, and (b) TechSpec lenses

The web strain measurement system comprises of a pair of GS3-U3-91S6M-C USB3.0 Grasshopper 9.1MP cameras, shown in Figure 4.3(a). The cameras are based on a Sony ICX814 sensor, 1" format, with $3.69 \mu\text{m}$ pixel size. The acquisition rate is 9 frames per second at $3376 \times 2704 \text{ pixel}^2$ resolution. The cameras are equipped with Tamron 23FM16SP lenses with a 16mm focal length (Figure 4.3b). Similarly to the TOR camera system, the pair of web cameras are mounted to a carbon fiber bar (19 inch length), which, in turn is attached to another articulated arm that is permanently attached to the cart.

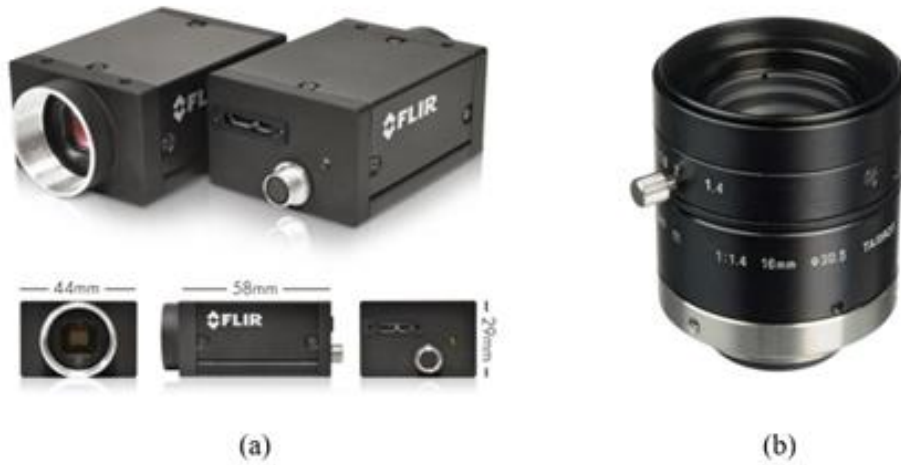


Figure 4.3: (a) GS3-U3-91S6M-C Grasshopper cameras, and (b) Tamron lenses



Figure 4.4: Carbon Fiber Bar

4.1.2 Thermal Camera

A handheld FLIR E6 Wi-I thermal camera is used to acquire a thermal surface scan of the rail and obtain temperature measurements of the rail during heating, seen below in Figure 4.5. The thermal camera has a resolution of 80 pixels by 60 pixels and an accuracy of +/- 2% of reading for ambient temperature in the range -4°F to 482°F for object temperature above freezing.



Figure 4.5: FLIR E6 Thermal Camera

4.1.3 Lighting

To achieve adequate and uniform lighting that is important in high quality images, two pairs of LED blue lights are mounted on the frame on flexible arms for easy adjustment when illuminating the TOR and Web. The lights used are EXZEIT brand waterproof 12/24V LED light bars. The lights are 6.3 inches in length and have a 120-degree flood range at 4000 lumens, shown in Figure 4.6a. The lights mounted on the frame are shown below in Figure 4.5b, and the brightness is controlled by individual dimmer switches. The blue lights are used in conjunction with blue light filters on the camera lenses to reduce the effects of shadows and reflections when imaging the rail surface in the field.



(a)



(b)

Figure 4.6: (a) LED lights, and (b) lights mounted on frame (circled in red)

4.1.4 System Calibration Targets

The camera systems, once the relative position is fixed, need to be calibrated in order to determine its geometric parameters before it is used in data acquisition. Calibration requires the use of a calibration target that consists of a rectangular grid of points of known size and spacing. Considering the camera configuration used for this application, and the recommendation that the target take up majority of the camera field of view (Standardization, 2018) (Figure 4.7), a 12x9 grid of 16 mm diameter circular dots is used.

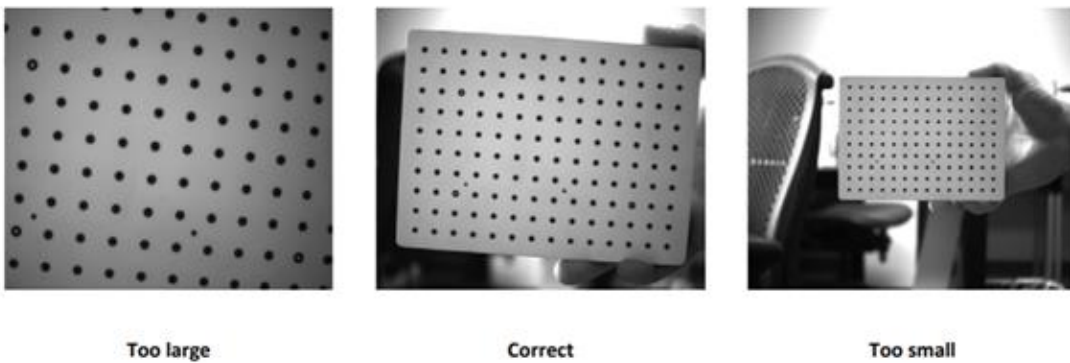


Figure 4.7: Calibration grid sizing

4.1.5 Rail Heating Equipment for Induced Heating Cycle

When an induced heating cycle is required, four Nemco 72-inch, 1725-watt infrared strip heaters are consecutively placed against the web of the rail. Although the area of interest is only located between two consecutive ties, more representative conditions of a natural heating cycle are obtained when a longer segment is heated. The heaters are shown below in Figure 4.8. It is observed that due to the current laboratory conditions, the heaters cannot be placed consecutively so instead they are staggered as shown in Figure 4.6b, while in the field all heaters are placed on the gage side.

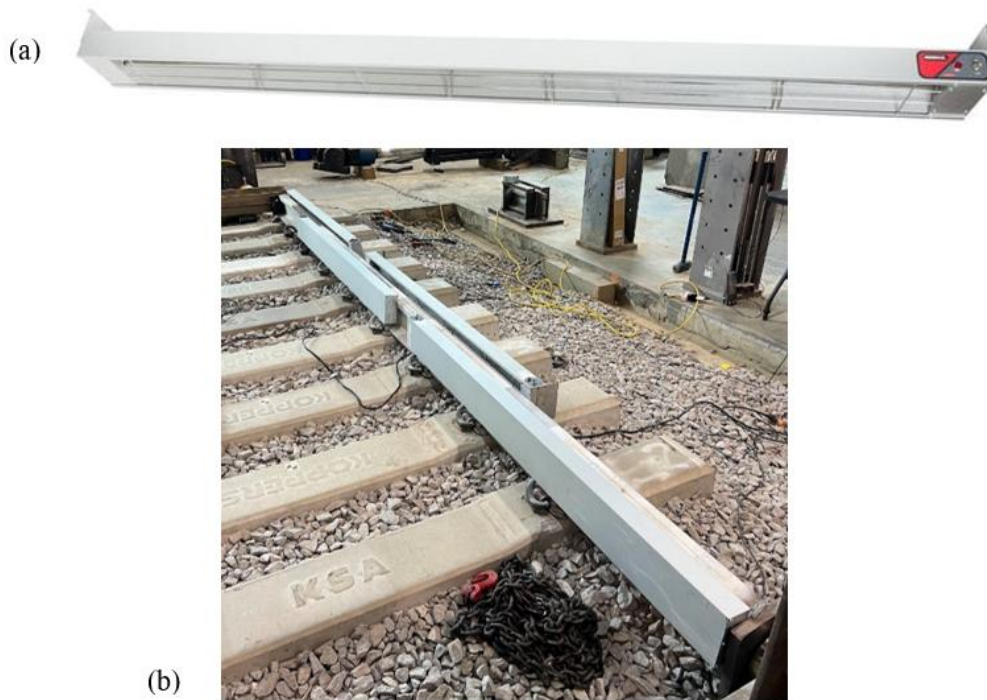


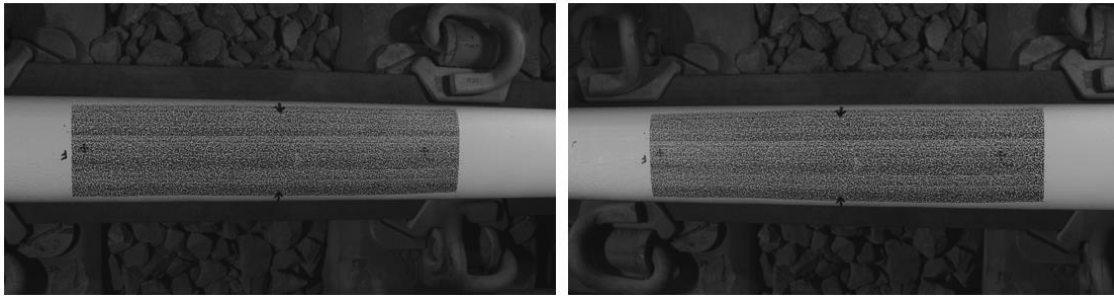
Figure 4.8: (a) Nemco 72" heating strip, and (b) lab configuration

4.2 System Configuration

Parametric studies have been performed in order to optimize the system parameters, including camera distances and angles, and speckle sizing.

4.2.1 Camera System

According to the DIC Good Practices guide, the ideal camera angle is between 15° - 30° (Standardization, 2018). For the top of rail and web, the distance from the cameras to the area of interest is approximately 20 inches and 18 inches, respectively. These distances position the cameras so that the area of interest between two consecutive ties takes up the majority of the field of view (Figure 4.9). For these given distances and the desired camera angles, the two cameras for each system are mounted approximately 2 inches apart (Figure 4.10). Calibration results indicate that this positioning results in a stereo-angle of approximately 25° .



(a)

(b)

Figure 4.9: TOR cameras field of view for (a) camera 0, and (b) camera 1



(a)



(b)

Figure 4.10: (a) TOR cameras, and (b) web cameras

4.2.2 Speckle Size

Investigation into the optimal speckle pattern has also been done. This included the testing of several different combinations of speckle sizes, randomization, and densities. A random speckle generator program was used to produce these patterns. Speckle patterns were created with sizes ranging from 0.50mm to 1.5mm, densities ranging from 30% to 90%, and randomization ranging from 40% to 90%. These patterns were then each individually imaged with the DIC camera system and analyzed, using the subset size and pixels to determine whether the pattern was optimal or not. Four different patterns were

analyzed for the top of rail, two with a speckle size of 0.75mm with two different density/variability combinations, and the other two with a 1.0mm speckle size with the same two different density/variability combinations, which can be seen below in Figure 4.11.

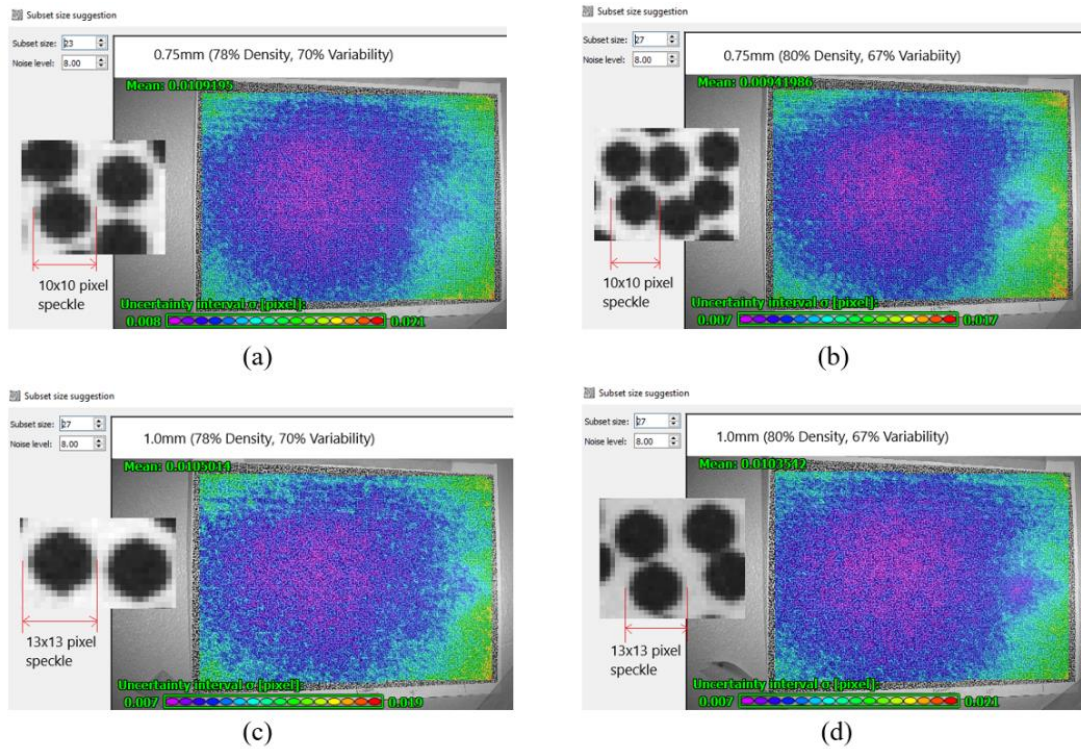


Figure 4.11: VID-3D Suggested Subset Size for (a) 0.75mm (78% Density, 70% Variability), (b) 0.75mm (80% Density, 67% Variability), (c) 1.0mm (78% Density, 70% Variability), and (d) 1.0mm (80% Density, 67% Variability)

For the top of rail, a speckle size of 0.75mm with 78% density and 70% variability (Figure 4.11a) was determined to be sufficient for the purposes of the application due to the lowest subset recommendation (23) and meeting the minimum pixel requirement.

For the web, four different patterns were analyzed, two with a speckle size of 1.0mm with two different density/variability combinations, and the other two with a

1.5mm speckle size with the same two different density/variability combinations, similar to the top of rail, which can be seen below in Figure 4.12.

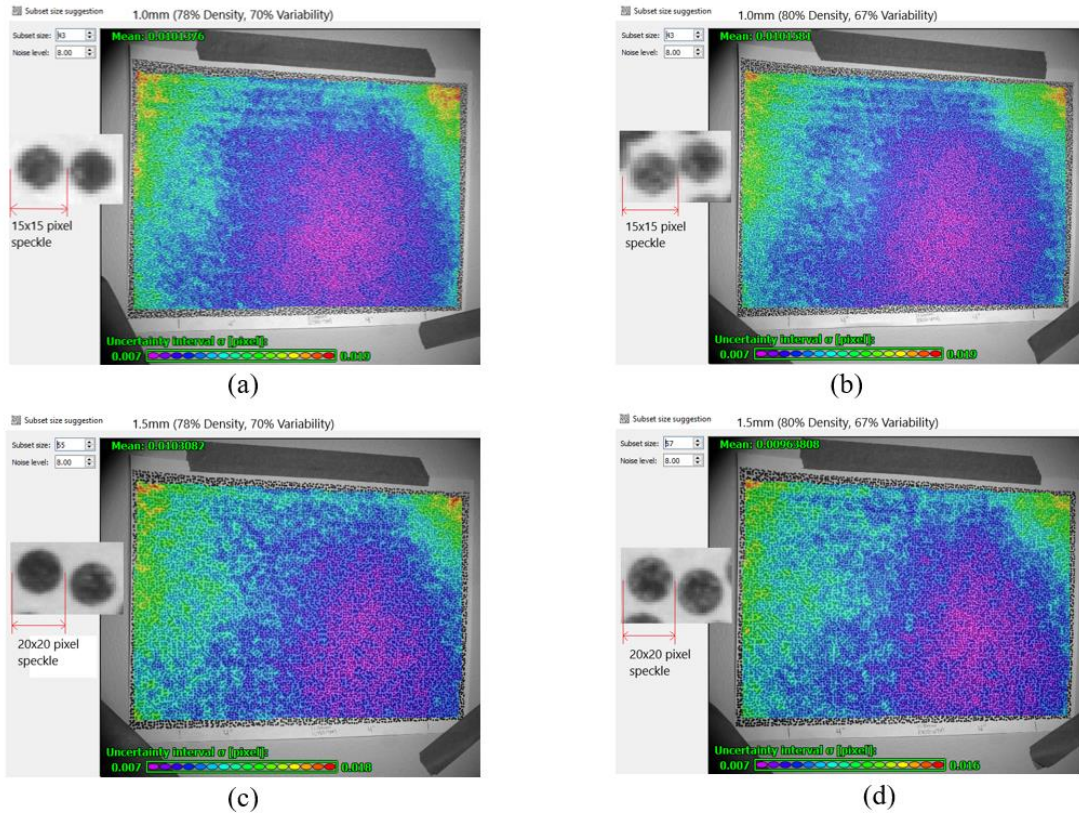


Figure 4.12: VIC-3D Suggested Subset Size for (a) 1.0mm (78% Density, 70% Variability), (b) 1.0mm (80% Density, 67% Variability), (c) 1.5mm (78% Density, 70% Variability), and (d) 1.5mm (80% Density, 67% Variability)

For the web, either of the patterns with a speckle size of 1.0mm were determined to be sufficient for the purposes of the application due to the lowest subset recommendation (43) and meeting the minimum pixel requirement. However, due to the laser printer shape being unable to print on the web, the current speckling method via stamp and ink pad are sufficient, with a speckle size on the stamp of 1.5mm.

4.3 Verification

In order to verify that the StereoDIC system is accurate, two separate analyses were performed to assess the accuracy of “flatness” measured by the system. To this end, a 6”x18”x2” granite slab milled flat with a tolerance of 0.00005 inches (0.00127 mm) is used in the verification studies (Figure 4.13).

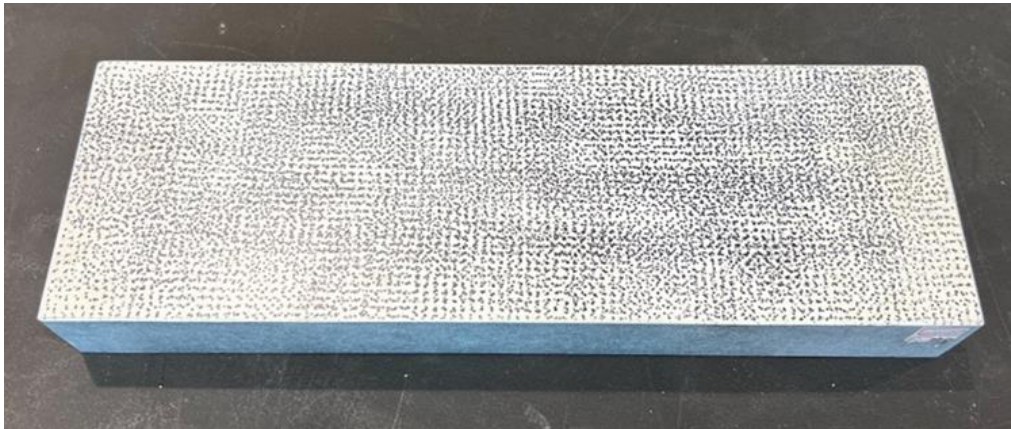
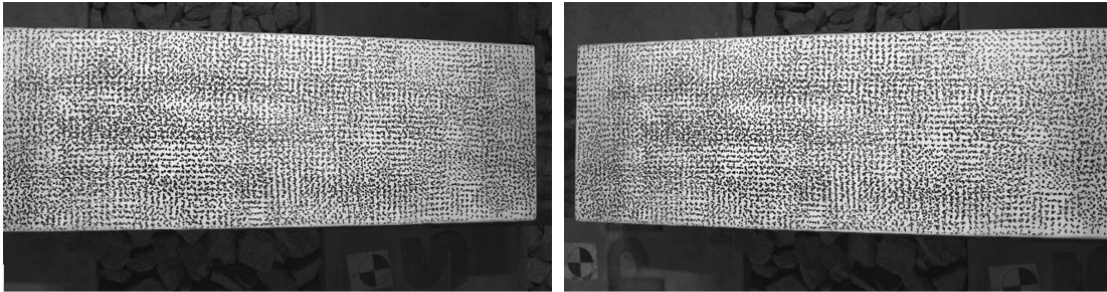


Figure 4.13: Granite slab

The first test was conducted on 10/13/2022. In this test the distance between the cameras and the slab was such that the slab took up the majority of the camera field of view, as shown in Figure 4.14, and 51 pairs of images were acquired. Subsequently, an average image is obtained by averaging the pixel intensity of the 51-image set. This average image was considered as the baseline for the correlation. Three profiles were extracted horizontally across the specimen, one each through the center, upper edge, and lower edge of the slab. This was to check for any radial distortion present in the extreme edges of the frame. The results agreed with the known flatness of the slab for all three profiles, with a noise range of -0.004 mm to 0.004 mm, or approximately 8 microns.

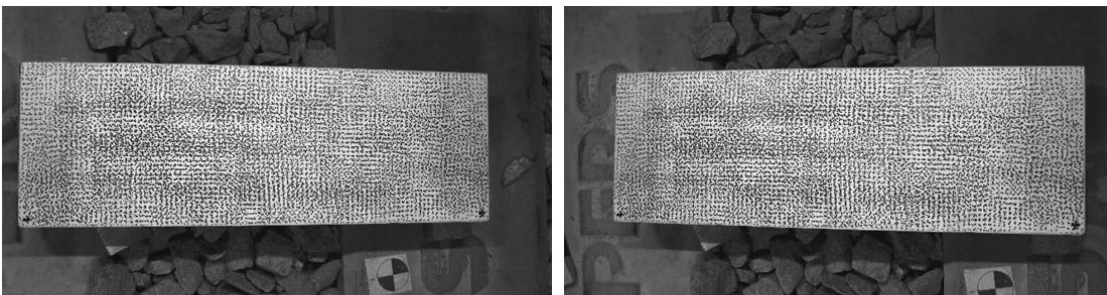


(a)

(b)

Figure 4.14: Field of view of (a) camera 0, and (b) camera 1

The second test was conducted on 10/21/2022. In this test the distance between the cameras and the slab was increased, placing the slab approximately at the center of the image, as shown in Figure 4.15, and 41 pairs of images were acquired. Subsequently, an average image is obtained by averaging the pixel intensity of the 41-image set. This average image was considered as the baseline for the correlation. A single profile was extracted horizontally across the specimen for each set. The results again agreed with the known flatness of the slab for all three profiles, with a noise range of -0.005 mm to 0.005 mm, or approximately 10 microns.



(a)

(b)

Figure 4.15: Field of view of (a) camera 0, and (b) camera 1

4.4 Acquisition Platforms

Two different data acquisition platforms were used in the field. The first is the rigid frame designed in Chao's work (Chao, 2022). This rigid frame, shown in Figure 4.16 below, allowed adjustments to be made in camera positioning before testing began and provided ample stability for the system once in place.



Figure 4.16: DIC Frame

The latest acquisition platform, shown below in Figure 4.17, was designed to allow the system to be more easily moved throughout testing. This new platform provides the ability to obtain measurements at more than one location during a single testing period. This is a major improvement to the overall testing procedure, as it now allows for multiple segments to be tested concurrently, providing more data to be analyzed and verified for RNT determination.



Figure 4.17: Rail Cart

Chapter 5 Data Acquisition and Processing

This chapter discusses procedures related to setting up the StereoDIC camera system, either in the lab, or for field measurements, followed by the data (image) acquisition process. The chapter concludes with the workflow for image processing for estimating RNT based on the current approach that limits acquisition from a static platform, and the proposed modification that allows for acquisition from a moving platform.

5.1 General Setup Procedure

The general StereoDIC testing procedure is described below.

5.1.1 Typical Equipment

Typical equipment required for a test includes items used to prepare the rail segment as well as equipment related to DIC. These items include:

Rail Cleaning: Acetone, rags/paper towels, wire brush.

Rail Speckling: Flat white spray paint, blue painter's tape, laser printer and/or stamp and ink pad, fine tip sharpies, ruler/tape measure.

StereoDIC Camera System: Cameras/lenses with filters, thermal camera, power supply, image acquisition software (VIC Snap), calibration grid, lighting.

Miscellaneous: Sun filters, heaters, extension cords, fan.

5.1.2 Site Preparation

Once a suitable testing segment has been determined, the setup process can begin. The rail is prepared first as listed following:

1. Wipe surface of rail clean of any debris or irregularities using acetone, rags/paper towels, and/or wire brushes. Allow surface to dry before moving to next step.
2. Using flat white spray paint, apply thin, even coats to rail surface (both TOR and Web) to apply a suitable white background to create the necessary contrast with the speckles, as shown in Figure 5.1. Allow paint to adequately dry to the touch before applying next coat(s), until surface is opaque.
3. Once the paint is dry, begin speckling using laser printer and/or stamp and ink pad. When using the laser printer, it is noted that three printer side-by-side passes along the length are needed to cover the full width of the top of rail with a 1-inch-wide printer head. To avoid printing over existing speckle strip, use the blue painter's tape to cover existing speckle and create a straight border line. Speckle may be corrected using sharpies to fill in gaps or correct mistakes. Speckled tie is shown in Figure 5.2.
4. After speckle pattern is sufficiently applied, use a sharpie and a ruler/tape measure to mark on the top of rail the location of the mid-point of the rail segment between ties, and the location of the tie edges.



Figure 5.1: (a) TOR and (b) web painted white

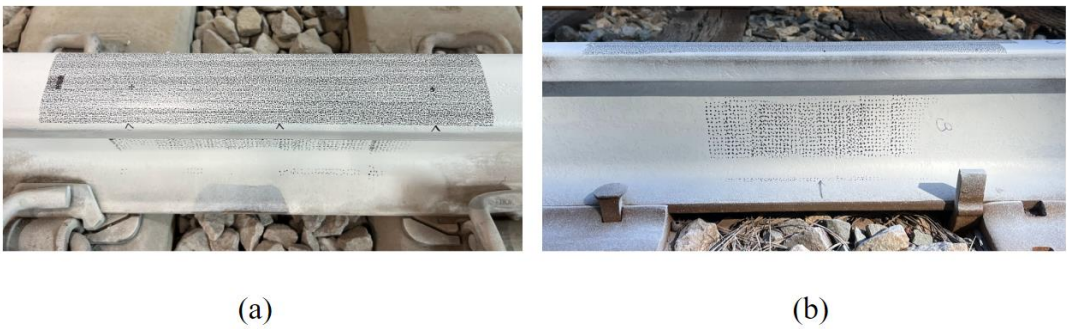


Figure 5.2: (a) TOR and (b) web speckled

5.1.3 StereoDIC Camera System Setup Procedure

To set up the DIC system, the general procedure is as follows:

1. Begin by turning on the computer system and connecting the cameras to the system to allow them to warm up for about 30 min before the testing starts.
2. Install cameras on acquisition platform.
3. Turn on lighting and adjust so that there are minimal reflections (reflections can be observed in VIC-Snap).
4. Using a calibration grid, obtain 20-40 calibration images. Make sure there are enough images so that all areas of the camera view are covered, and all orientations and angles are captured as well. Do this for both the top of rail

cameras and the web cameras. See DIC Good Practices for detailed calibration instructions.

5. Verify calibration images in VIC-3D by loading calibration images to the software and perform calibration. Although a calibration score below 0.9 is acceptable, a value of 0.7, or less, typically produces better correlations.

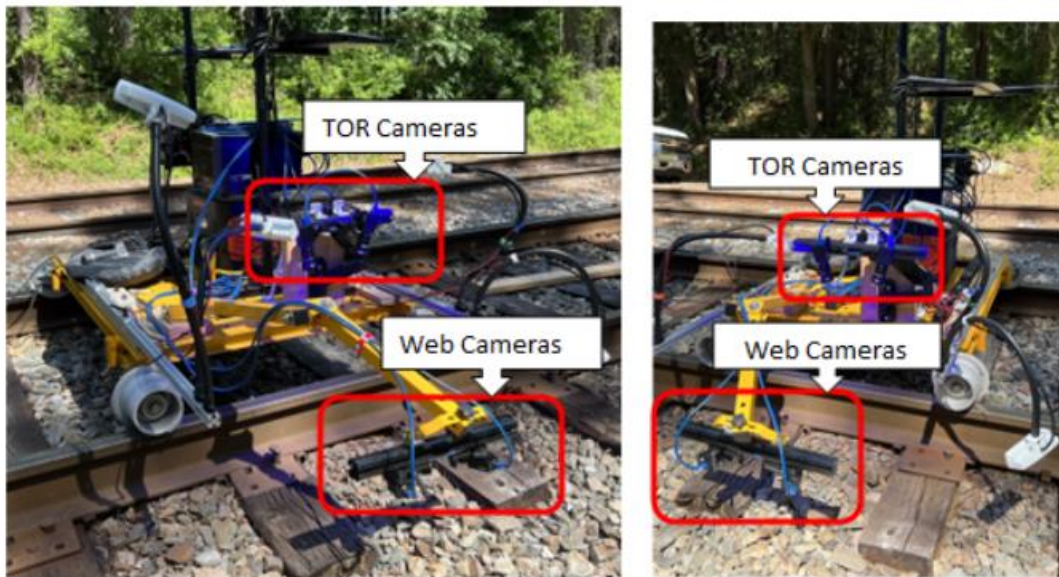


Figure 5.3: Location of cameras mounted to frame and rail cart (circled in red)

5.2 Testing Procedure and Image Acquisition

Once the system is set up, the test can begin. The testing procedure steps are below.

1. If the test being performed requires an induced heating cycle, at least 3 heaters (for a total length of 18 feet) should be placed against the web of the rail consecutively and centered around the area of interest.
2. A first set of images is taken, and the corresponding temperature of the TOR and web at that time should be recorded as well. A minimum of 20 images should be taken, though as many as 40 images is recommended.

3. Turn on the heaters to begin the heating process. Data acquisition (images and temperatures) should be done in 5-10°F increments.
4. Once the rail has reached around 140°F, or the maximum desired temperature, the heaters should be turned off and removed from the web.
5. Data acquisitions can also be taken during cooldown.

5.3 Data Processing

5.3.1 Correlating Across Temperatures

Once the test has been completed, post processing can be done. One important aspect of the testing process is that the system cannot move throughout the duration of the test. By allowing the system to remain in the same position throughout the heating process, the data processing can be done by correlating the images across temperatures. For each data set, an average image is obtained by averaging the intensity pixel-by-pixel over all images in the set. This is done to reduce any noise that might be present in the individual images. Once a single averaged image is obtained for each temperature, the image set 0 is set as the baseline image. All subsequent averaged images for each set are used in calculating deformations with respect to baseline average image. An optimal subset size is determined by ensuring that the minimum of a 3x3 pixel grid is enclosed within a subset area. The suggested subset size in the VIC-3D program is sufficient but may be increased if the image quality is not ideal. Typically, the step size is left as 7, but may also be increased if problems are encountered when processing the data. Increasing the subset size and step size are ways to improve a high projection error score, but reduces the resolution of the measurements. When processing the data, the lowest projection

error is ideal and any data sets that contain a high projection error may need to be discarded as it is unreliable. If the projection errors are consistent among data sets, the data may still be usable. Once all data is processed, the curvature of the top of rail at each temperature can be extracted and the temperature-curvature plot created.

5.3.2 Shape Measurements and Correlation within a Single Temperature

A significant improvement to the RNT testing method was made when moving the acquisition system from the stationary rigid frame to a moving platform (rail cart). By allowing the system to move along the track throughout the duration of a single test, multiple locations can be measured in a single test, and the need for the speckle pattern to remain intact throughout the test is no longer necessary. By processing the data by extracting the shape from a single temperature independently from other data sets, the speckle pattern remaining undisturbed between temperature sets is no longer of concern. However, the shape in each case is determined with respect to a different coordinate system for each temperature, and not with respect to a common coordinate system where image correlation takes place across temperatures. As long as the camera system is not disturbed during acquisition at a single temperature, the data is usable. This new processing approach facilitates better quality control since image correlation of images before averaging within a single temperature provides an assessment of the noise. A shape measurement is taken from each image within a single data set, and the variability between all images can be used to filter outliers in the data as well as aid in the determination of an unusable data set. Once a single, average shape measurement is determined for each temperature individually, all temperature-curvatures for the given segment can be plotted to then determine the RNT.

Chapter 6 Field Implementation & Parametric Studies

This chapter discusses field tests performed in 2022 and 2023. There have been several variations of field testing done since Chao's work. Three days of field testing were done in June of 2022, and another two days in April of 2023. Table 6.1 below provides a brief summary of the various test conditions for each day of testing. A description of the test objectives, conditions, and results are included in each section for each day of testing. Discussions regarding the quality of results and suggestions for future work will be in the following chapters.

6.1 Test Site

All field tests were conducted at the same site, located near a grade crossing off Alpine Road in Columbia, SC. This location has 118RE sized rail with timber ties and a desired RNT for this region of 105°F.

6.2 RNT Test Objectives

The objectives of all field testing were to investigate how changing various parameters of the testing equipment and procedures would affect the quality of results. In 2022, the DIC camera frame was used. The first day of testing followed the procedure that was used in Chao's work and utilized an induced heating cycle. The second day, the rail was allowed to heat naturally over several hours, and the last day the frame was moved

between data acquisitions. Testing performed in 2023 implemented the use of the rail cart, and the rail heated naturally for all days of testing. The first day, three segments of rail were tested, and day two tested another three different segments. Table 6.1 below provides a brief summary of the conditions for each test. Each day of testing is discussed in more detail below.

Table 6.1: Field Test Conditions

Test	Date	Station or Segment	Induced Heating	Natural Heating	Additional Anchors	Frame	Cart	TOR Results Quality	WEB Results Quality	Comments
1	6/7/2022	Station 1	x			x		Poor	Poor	Low correlations, minimal constraints
2	6/7/2022	Station 2	x			x		Poor	Fair	Web shows some constraint
3	6/8/2022	N/A		x		x		Fair	Good	TOR high PE (camera bar expansion), web shows some constraint
4	6/9/2022	N/A	x		x	x		Good	Good	Frame movement on/off track, anchors improve constraint
5	4/20/2023	A0		x			x	Poor	Fair	High PE, web out of focus
6	4/20/2023	B0		x			x	Fair	Fair	High PE, web out of focus
7	4/20/2023	C0		x			x	N/A	N/A	Not enough data
8	4/21/2023	D0		x			x	Fair	Good	Low correlation
9	4/21/2023	E0		x			x	Good	Good	Good correlation and constraints
10	4/21/2023	F0		x			x	Fair	Good	Limited data

6.2.1 Field Tests 1 and 2

6.2.1.1 Test Conditions

For this day of testing, two separate experiments were performed. The first test was performed on a segment of rail that had been previously tested a year prior by Chao (referred to as Station 1). The web speckle was still visible, so it was wiped of any surface debris and otherwise left as is. Station 2 was located at a different segment of the track and was a new speckle for the web.

6.2.1.2 RNT Measurements for Station 1

A total of ten data sets were obtained, starting at 76.5°F and ending at 139°F using an induced heating cycle. For the top of rail analysis, three different techniques were used in determining the RNT from the extracted data. First, an analysis was performed, as previously in Chao's work, using the averaged images and finding the deformation based off the "set 0" data (analysis labeled as "full analysis" below). The second technique, called "alt analysis," was completed by analyzing all images in each data set in VIC-3D. The values of curvature, k , for all images were then extracted and averaged. This average curvature was then plotted versus the corresponding temperatures. The standard deviation of the k values for each data set was also observed. The third technique, "alt reduced analysis," attempted to filter outliers from the data by organizing all the curvatures in a histogram removing any values that were greater than one standard deviation. Each of these analyses were plotted and a best fit line was drawn, where the point of zero curvature is the RNT. Results from these analyses can be seen below in Figure 6.1.

6-7-2022 Station 1

Set	TOR (°F)	Regular Full Analysis				Alt Analysis				Alt Reduced Analysis			
		Proj Error	Subset	# Images	k	Proj Error	Subset	# Images	k (avg)	St Dev	# Images	k (avg)	St Dev
0	76.5	0.33-0.87	31	1(avg)	0.2003	0.048	31	52	-0.4908	0.9855	44	-0.5694	0.5134
1	89.4			1(avg)	-0.2332	0.034	37	52	-1.8676	2.2884	29	-1.3449	1.0435
2	96.3			1(avg)	0.0032	0.068	33	52	-1.4908	1.4837	39	-1.7967	0.7553
3	103			1(avg)	0.3404	0.075	35	40	-0.6671	2.4511	30	-0.6008	1.0829
4	109			1(avg)	0.1429	0.076	37	52	-2.5853	1.7720	39	-2.5853	0.8539
5	115			1(avg)	0.0933	0.085	33	52	-0.7956	0.7813	47	-0.8939	0.6288
6	119			1(avg)	-0.4653	0.068	33	52	-2.6468	0.8261	42	-2.3001	0.3930
7	123			1(avg)	-0.1610	0.078	33	53	-2.3096	1.5171	40	-2.0484	0.9989
8	128			1(avg)	0.2313	0.071	33	52	-1.3411	5.1673	22	-1.9418	0.7810
9	134			1(avg)	0.3362	0.067	35	52	-1.0894	3.0135	28	-1.2275	0.8381
10	139	1(avg)	-0.5639	0.059	35	52	-1.8090	1.5689	45	-2.0227	0.8340		

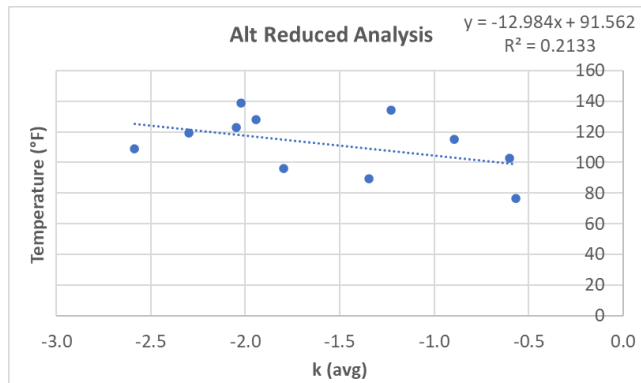
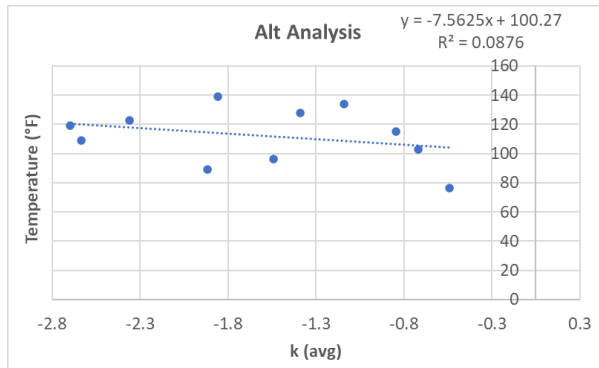
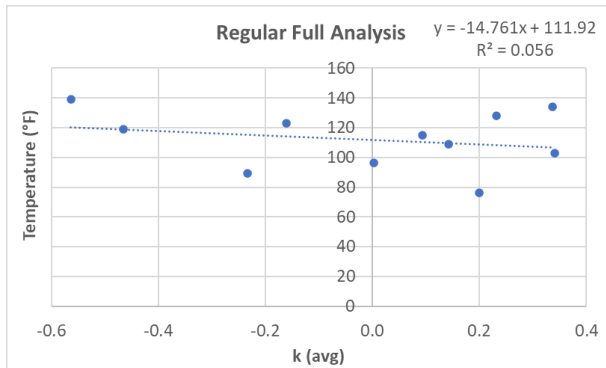


Figure 6.1: Test 1 Station 1 TOR Results

For the web analysis, a single image pair for sets 1-10 were analyzed, and the relevant data was extracted. Set 0 image quality was poor and therefore disregarded. Further discussion on image quality can be found in Chapter 7. The e1 and e2 values were plotted versus the change in temperature, which can be seen below in Figure 6.2.

Set	ΔT (°F)	e1	e2
1	0	0.00	0.00
2	9.6	152.53	27.56
3	11.7	179.07	43.84
4	20.5	342.37	29.48
5	24.5	235.83	99.46
6	28.5	327.57	149.51
7	33.5	334.08	177.40
8	39.5	380.85	226.47
9	42.5	424.67	240.72
10	44.5	338.44	191.32

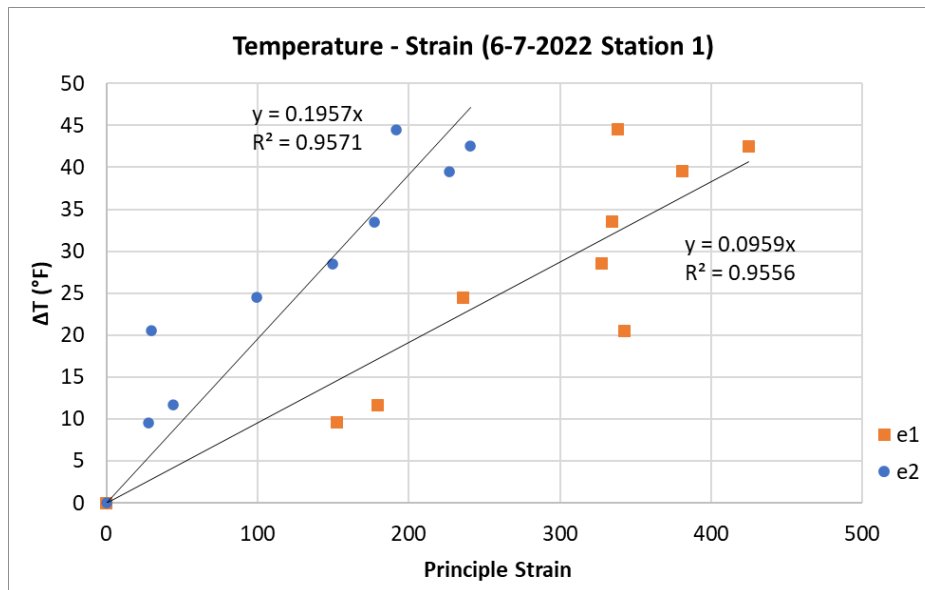


Figure 4: Test 1 Station 1 Web Results

6.2.1.3 Results Summary for Station 1

The top of rail analysis results shows a wide range of estimated RNT values (91°F-112°F), with very low correlation. Although each alternative analysis improved the correlation slightly, the overall analysis results do not appear to be reliable. The web

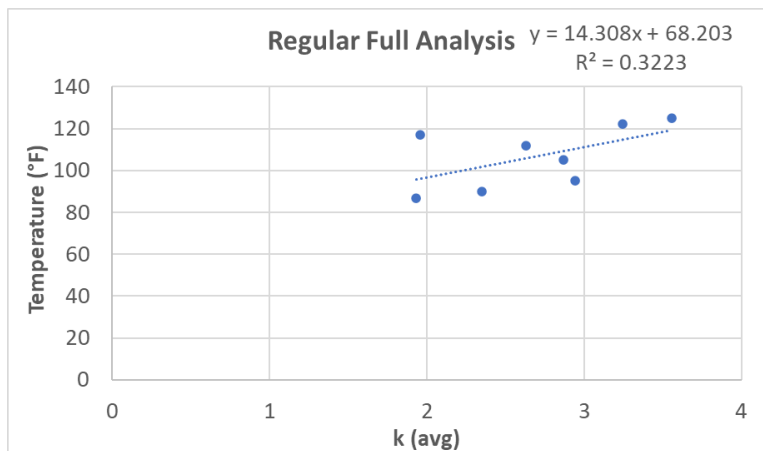
strain analysis shows minimal longitudinal constraints, which may explain the low correlation of the top of rail analysis. Strong conclusions should not be drawn from this data set.

6.2.1.4 RNT Measurements for Station 2

For Station 2, a total of seven data sets were obtained, starting at 86.7°F and ending at 125°F using an induced heating cycle. For the top of rail analysis, the same three processing techniques used for Station 1 were used in determining the RNT from the extracted data. It is noted that for sets 6 and 7, the projection errors were large and therefore the data was not considered in the RNT estimation. Results are seen below in Figure 6.3.

6-7-2022 Station 2

Set	TOR (°F)	Regular Full Analysis				Alt Analysis					Alt Reduced Analysis		
		Proj Error	Subset	# Images	k	Proj Error	Subset	# Images	k (avg)	St Dev	# Images	k (avg)	St Dev
0	86.7			1 (avg)	1.9318	0.009	35	52	1.5009	0.7543	48	1.4772	0.5660
1	90.1			1 (avg)	2.3473	0.019	31	52	5.0134	2.2797	33	4.8811	0.7850
2	95.2	0.008-		1 (avg)	2.9440	0.036	29	52	2.7463	3.5564	21	3.2992	1.2099
3	105	0.040	35	1 (avg)	2.8694	0.035	33	52	2.6502	1.8875	39	2.5284	0.8307
4	112			1 (avg)	2.6320	0.038	29	52	5.2365	1.5797	38	5.1782	0.9562
5	117			1 (avg)	1.9587	0.038	35	52	1.9309	1.4172	42	2.1375	0.8554
6	122	0.108-		1 (avg)	3.2442	0.1+	-	-	-	-	-	-	-
7	125	0.103	1 (avg)	3.5556	0.1+	-	-	-	-	-	-	-	



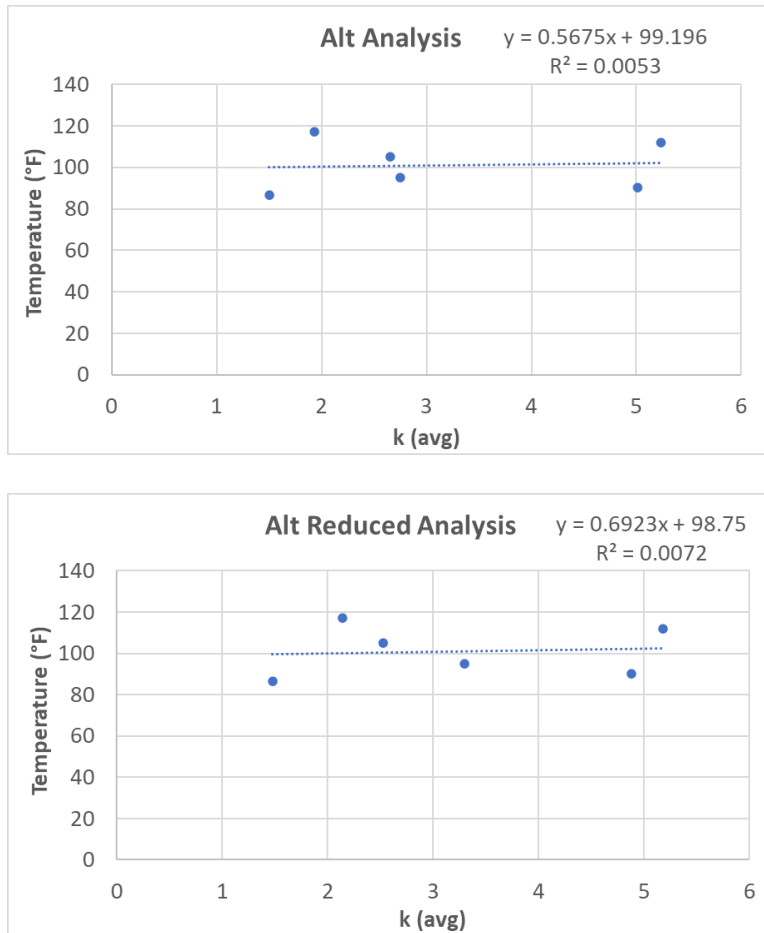


Figure 5: Test 2 Station 2 TOR Results

For Station 2 web, the averaged image for each data set was used. The results can be seen below in Figure 6.4.

6-7-2022 Station 2			
Set	ΔT (°F)	e1	e2
0	0	0.00	0.00
1	5	195.17	25.50
2	8.6	233.58	26.07
3	16.8	188.81	15.90
4	23.8	335.47	78.48
5	25.8	375.42	114.21
6	29.8	359.19	113.24
7	34.8	377.06	118.80

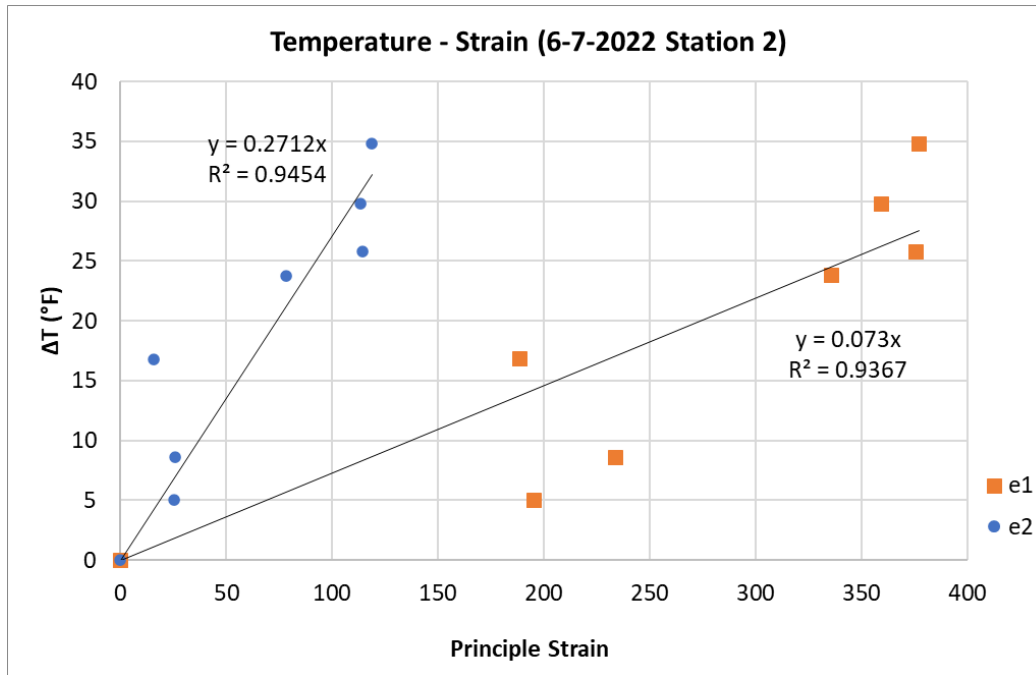


Figure 6: Test 2 Station 2 Web Results

6.2.1.5 Results Summary for Station 2

The analysis results show a wide range of estimated RNT values (68°F-99°F), with very low correlation, similar to Station 1 results. Efforts to improve the quality of the results using the alternative methods that improved Station 1’s results show the opposite for Station 2, with decreasing correlation. This could be due to the large standard deviations in the individual data sets. Better longitudinal constraints are observed in the web compared to Station 1. The poor results for the top of rail might be due to errors during data acquisition. Strong conclusions should not be drawn from this data set.

6.2.2 Field Test 3

6.2.2.1 *Test Conditions*

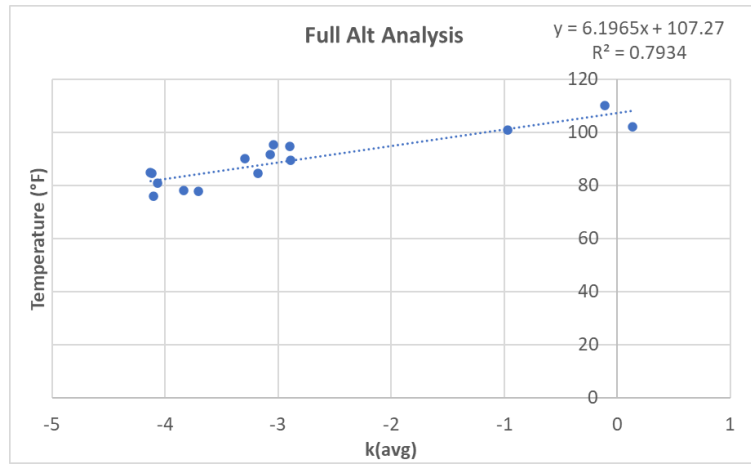
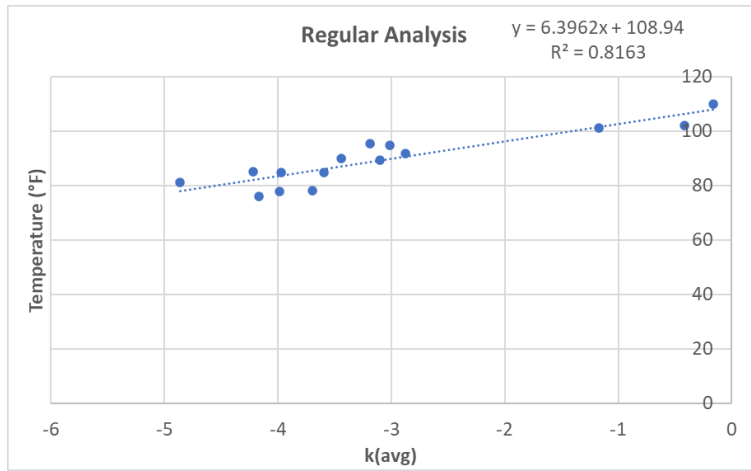
For day two of testing, a different segment from the previous day was tested. This day, the rail was allowed to heat naturally over several hours for the first time. By allowing the rail to heat naturally, a more uniform heating across the length of the rail can be achieved. This results in better longitudinal constraints, which can be observed in the web analysis.

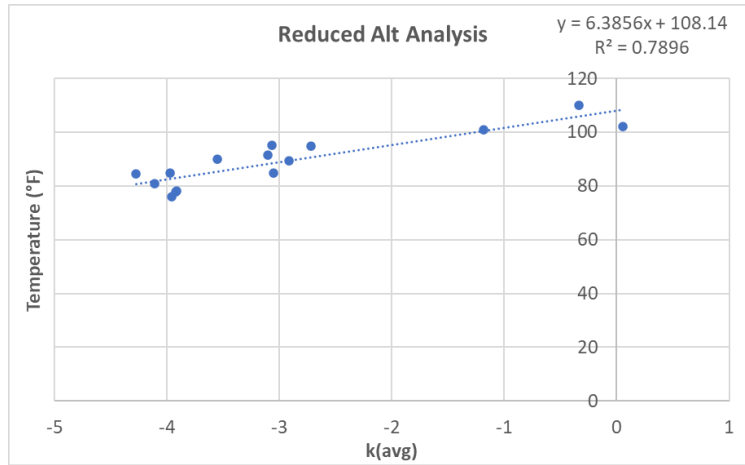
6.2.2.2 *RNT Measurements for Test 3*

A total of 14 data sets were obtained, starting at 81°F and ending at 110°F. For the top of rail analysis, the same three processing techniques as the previous day were again used to determine the RNT from the extracted data. It is noted that for all data sets, the projection error continuously increases. It is hypothesized that this could be the result of the aluminum bar the cameras are mounted on expanding as the temperature increases. Results are seen below in Figure 6.5a. Due to the temperature change being relatively small between each data set, similar temperatures across several sets were averaged, along with the corresponding curvatures averaged, resulting in four data sets which can be seen in Figure 6.5(b).

6-8-22 TOR

Set	TOR (°F)	Proj Error	Subset	Regular Analysis			Full Alt Analysis			Reduced Alt Analysis			
				# Images	k(avg)	Proj Error	Subset	# Images	k(avg)	St Dev	# Images	k(avg)	St Dev
0	81.0	0.038	31	1 (avg)	-4.8579	0.036-0.039	33	52	-4.0678	0.2816	45	-4.1143	0.226
1	75.9	0.120		1 (avg)	-4.1631	0.116-0.224	29	52	-4.0988	0.9861	43	-3.9574	0.5758
2	77.7	0.140		1 (avg)	-3.9805	0.136-0.144	29	52	-3.7031	1.0895	42	-3.9249	0.7496
3	78.1	0.195		1 (avg)	-3.6920	0.195-0.198	27	52	-3.8314	0.6351	49	-3.9189	0.5323
4	84.7	0.228		1 (avg)	-3.5914	0.226-0.232	27	52	-3.1769	0.9921	41	-3.0509	0.4773
5	84.9	0.204		1 (avg)	-4.2184	0.201-0.209	31	52	-4.1297	1.3394	43	-3.9749	0.5835
6	84.6	0.200		1 (avg)	-3.9688	0.199-0.203	29	52	-4.1195	0.8726	44	-4.2752	0.5479
7	90.0	0.237		1 (avg)	-3.4394	0.233-0.240	31	53	-3.292	1.2767	41	-3.5562	0.7043
8	89.4	0.274		1 (avg)	-3.1014	0.271-0.278	29	52	-2.8877	1.0053	46	-2.918	0.7335
9	91.6	0.295		1 (avg)	-2.8774	0.291-0.300	27	52	-3.0719	0.9436	42	-3.1006	0.5529
10	94.8	0.304		1 (avg)	-3.0138	0.302-0.309	29	52	-2.8926	1.5068	40	-2.718	0.8231
11	95.2	0.309		1 (avg)	-3.1827	0.308-0.311	31	52	-3.0416	0.9846	40	-3.0672	0.5923
12	101	0.454		1 (avg)	-1.1694	0.448-0.462	29	52	-0.9701	1.751	37	-1.1857	1.751
13	102	0.488		1 (avg)	-0.4187	0.484-0.494	29	52	0.1324	1.1796	45	0.0542	0.8281
14	110	0.566		1 (avg)	-0.1596	0.536-0.579	31	52	-0.1128	1.8247	38	-0.3368	1.0065

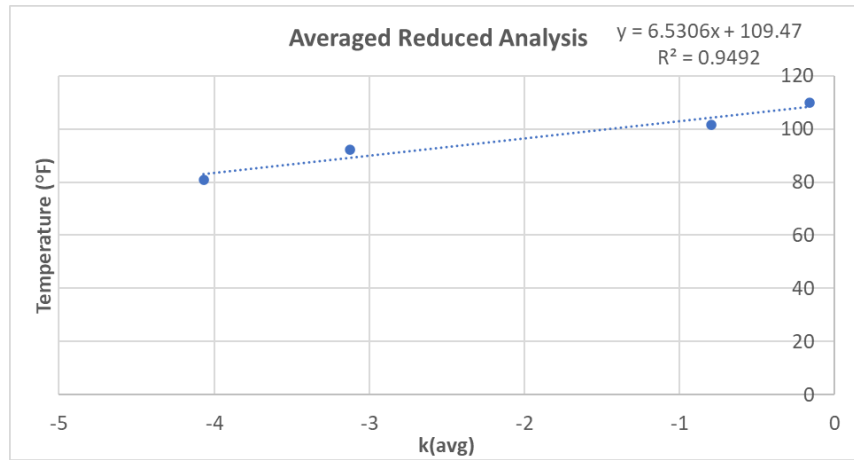




(a)

Averaged Reduced

Sets Avg'd	Avg TOR (°F)	Avg k
0 to 6	81	-4.0674
7 to 11	92.2	-3.1229
12 to 13	101.5	-0.7941
14	110	-0.1596

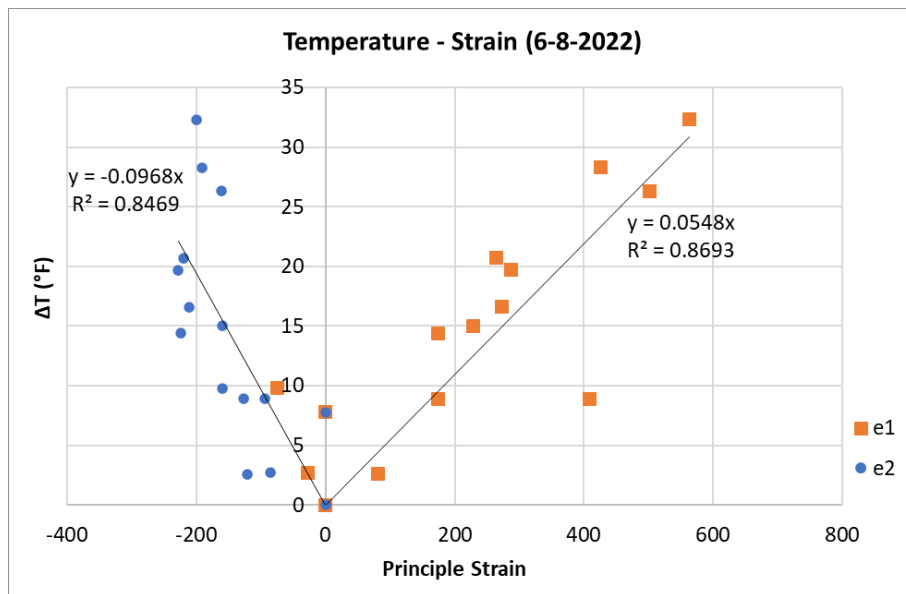


(b)

Figure 7: Test 3 TOR Results (a) all, and (b) Averaged Reduced Temperature - Curvature Results

For the web analysis, all data sets were analyzed using the averaged images, and the data sets were rearranged so that the temperatures were in an increasing order. The relevant data was extracted, and the e1 and e2 values were plotted versus the change in temperature, which can be seen below in Figure 6.6a. Figure 6.6b shows a reduced number of data sets, which show similar or better correlation.

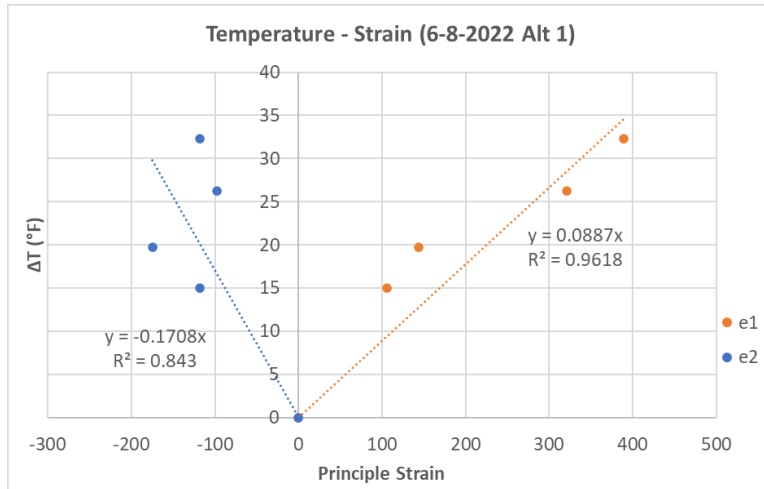
6-8-2022 Web (All)			
Set	ΔT (°F)	e1	e2
1	0	0	0
3	2.6	80.92	-121.70
2	2.7	-28.26	-84.88
0	7.8	0.00	0.00
4	8.9	174.80	-93.93
6	8.9	408.95	-127.20
5	9.8	-75.02	-160.37
8	14.4	174.21	-224.34
7	15.0	228.35	-160.51
9	16.6	272.17	-210.97
10	19.7	287.72	-228.37
11	20.7	264.34	-220.20
12	26.3	502.09	-161.28
13	28.3	425.69	-191.36
14	32.3	563.89	-199.84



(a)

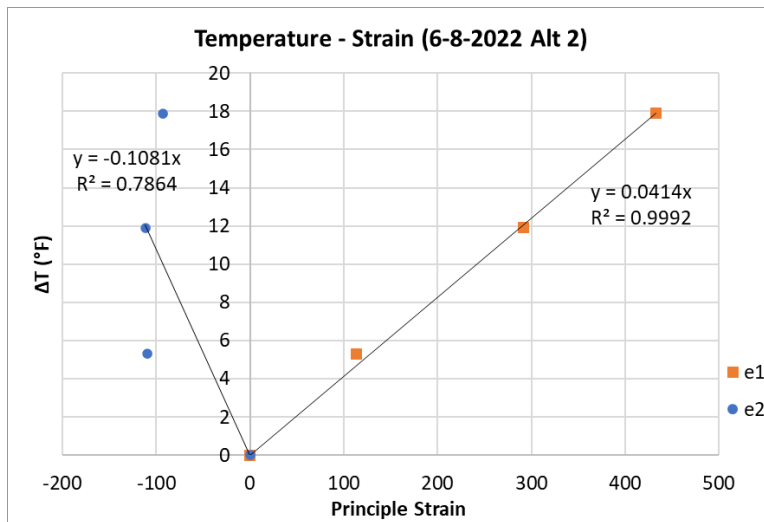
6-8-2022 Web Alt 1

Set	ΔT (°F)	e1	e2
1	0	0.00	0.00
7	15	105.68	-117.99
10	19.7	143.80	-174.56
12	26.3	321.03	-97.38
14	32.3	389.67	-118.27



6-8-2022 Web Alt 2

Set	ΔT (°F)	e1	e2
7	0	0.00	0.00
10	5.3	113.54	-109.39
12	11.9	291.87	-111.49
14	17.9	432.45	-92.69



(b)

Figure 8: Test 3 Web Results (a) all, and (b) Reduced Temperature - Strain Results

6.2.2.3 Results Summary for Test 3

The analysis results show a smaller range of estimated RNT values (107°F-110°F), with improved correlation. The averaged reduced results show an improvement in correlation and offer another possible alternative processing method. The web analysis shows decent longitudinal constraints as well. From this day of testing, the natural heating cycle is shown to be a promising alternative to induced heating.

6.2.3 Field Test 4

6.2.3.1 Test Conditions

For this day of testing, the camera frame was moved on and off the segment of track being tested. Additional rail anchors were added to the adjacent ties on each side of the tested segment (12 ties total), and the heating method was an induced cycle.

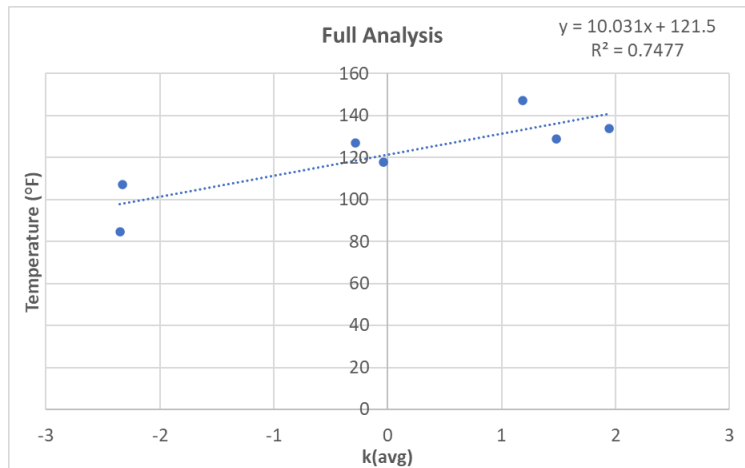
6.2.3.2 RNT Measurements for Test 4

Due to the frame being moved between data sets, the “regular analysis” done for the first two days of testing is not applicable for this data. So, three different techniques were used in determining the RNT from the extracted data. First, a “full analysis” was performed using all images that were obtained and processed in VIC-3D for shape measurements. The curvatures for each image were extracted and an averaged value was obtained. The average curvature and corresponding temperature were then plotted to find the estimated RNT. The second technique, “reduced analysis,” attempted to filter outliers in the data by observing the line slice extraction plot in VIC-3D and removing any outliers manually from the data. The number of images kept was noted and again the average curvature was plotted with temperature. The third technique, “alt reduced

analysis,” again attempted to filter outliers from the data by plotting all curvatures in a data set into a histogram and removing any outliers until the standard deviation was less than 1. It is noted that for sets 7 and 8 the projection errors were excessive, therefore the data was disregarded in the RNT estimation. Each of these analyses were plotted and a best fit line was drawn, where the y-intercept shows the RNT. The results can be seen below in Figure 6.7.

6-9-2022 TOR

Set	TOR (°F)	Proj Error	Subset	Full Analysis			Reduced Analysis			Alt Reduced Analysis		
				# Images	k(avg)	St Dev	# Images	k(avg)	St Dev	# Images	k(avg)	St Dev
0	84.6	0.01	29	52	-2.3502	0.4688	42	-2.4146	0.3900	48	-2.3974	0.3677
1	107	0.072	31	42	-2.3304	2.1257	26	-2.3710	1.2359	28	-2.2574	0.7433
2	118	0.082	29	42	-0.0408	0.6934	27	0.0418	0.5228	39	-0.0397	0.5137
3	129	0.01	33	42	1.4809	1.5551	15	1.3198	0.9052	27	1.4901	0.6151
4	134	0.093	35	42	1.9461	1.6743	20	1.6826	0.9926	28	1.5124	0.7209
5	147	0.055	33	42	1.1826	3.3554	21	1.9487	1.4054	22	1.8997	0.8304
6	127	0.012	33	42	-0.2806	2.1640	25	-0.2799	1.3602	21	0.2944	0.7676
7	122	2.xx	-	-	-	-	-	-	-	-	-	-
8	120	-	-	-	-	-	-	-	-	-	-	-



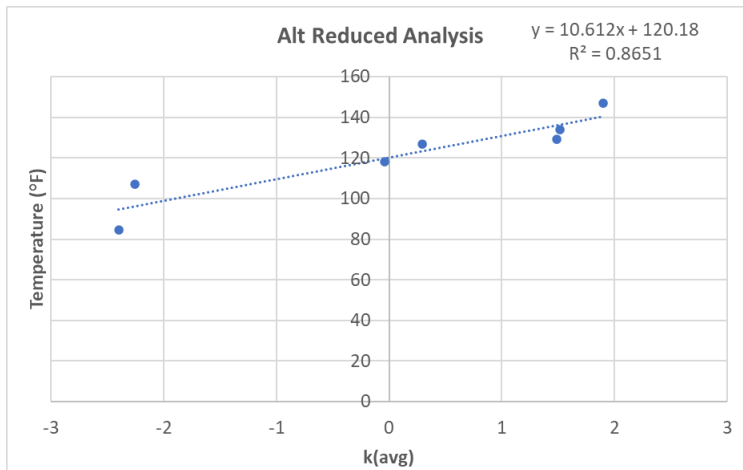
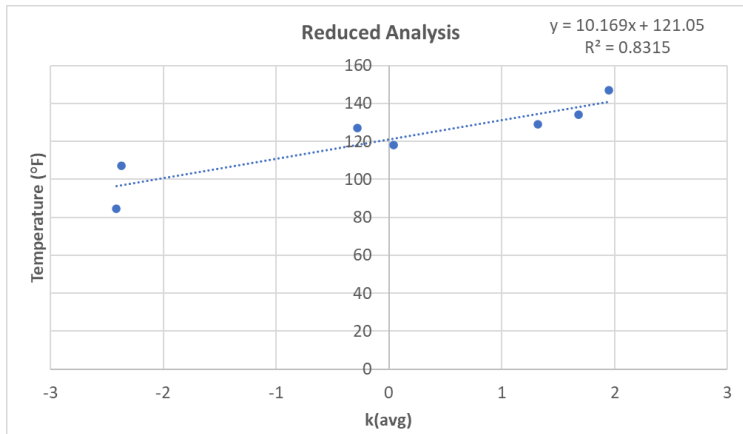


Figure 9: Test 4 TOR Results

The web was analyzed using the averaged image for each data set. The results can be seen below in Figure 6.8.

6-9-2022 Web			
Set	ΔT (°F)	e1	e2
0	0	-8.9E-12	-2E-11
1	19.4	364.001	121.924
2	33.4	355.861	101.312
3	47.4	614.54	217.64
4	49.4	806.57	166.54
5	61.4	897.53	236.98
6	43.4	693.61	106.82
7	38.4	668.37	49.20
8	36.4	513.716	55.8

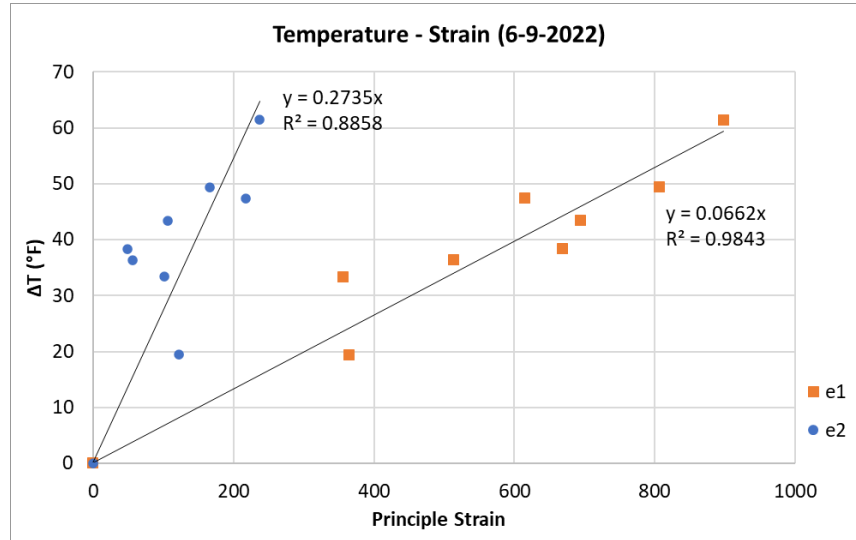


Figure 10: Test 4 Web Results

6.2.3.3 Results Summary for Test 4

The analysis results show a very small range of estimated RNT values (120°F-121°F), with good correlation. The web analysis shows good longitudinal constraints, as well as higher strains. From this day of testing, RNT estimation based on only shape measurements, as opposed to correlating across temperatures, is validated. It is also concluded that additional rail clips improve results.

6.2.4 Field Tests 5, 6, and 7

6.2.4.1 *Test Conditions*

For this test, three segments of rail were tested, and the heating method was a natural heat cycle. This is also the first time the rail cart is being used in the field. The three segments tested are identified as segment A0, B0, and C0. For all top of rail analysis, all images obtained were processed and shape measurements extracted. All curvatures were averaged together and plotted with temperature. It should be noted that one of the web cameras was out of focus during all data acquisition on this day, therefore affecting the quality of the web results. Further discussion on image quality can be found in Chapter 7.

6.2.4.2 *RNT Measurements for Test 5 (Segment A0)*

At segment A0, three sets of data were collected for the top of rail and two for the web, between 78.1°F and 88.5°F. The standard deviation was used as a reference to remove outliers in the data until the value reduced to below one for the top of rail analysis. Both analyses, all data and reduced data, were plotted. Results can be seen below in Figure 6.9.

Segment A0			All Data		Reduced Data	
Set	TOR (°F)	PE	k (1/mm)	St Dev	k (1/mm)	St Dev
0	78.1	1.14	4.6120	0.9130	4.6120	0.9130
1	85	1.16	5.6576	1.0415	5.5618	0.9666
2	88.5	0.528	6.2596	1.5995	6.1736	0.9880

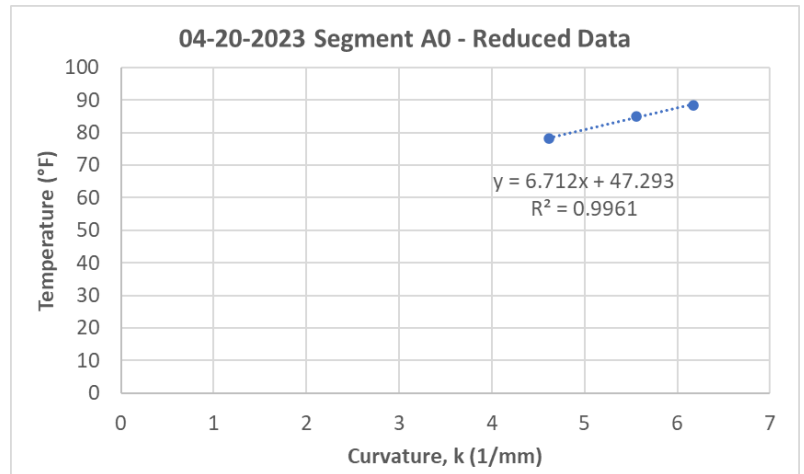
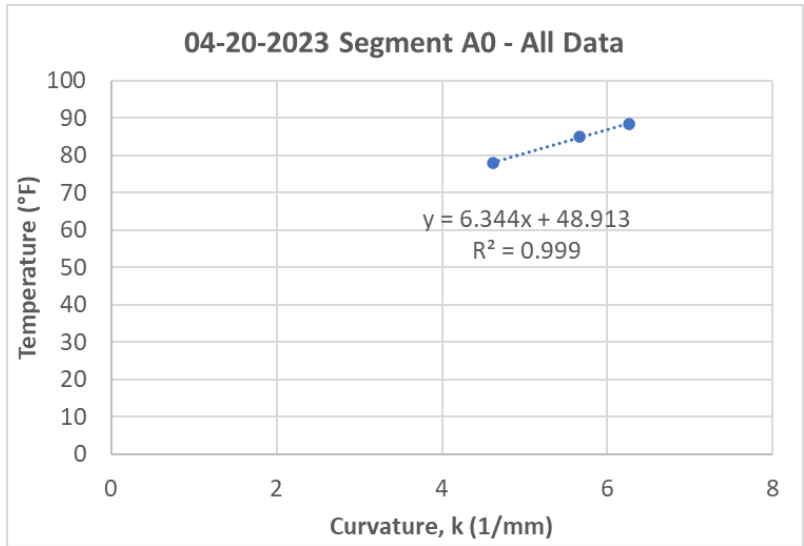


Figure 11: Test 5 (Segment A0) TOR Results

Segment A0 web analysis can be seen below in Figure 6.10.

Set	ΔT (°F)	e1	e2
0	0	0.00	0.00
1	5.9	-63.23	-355.55

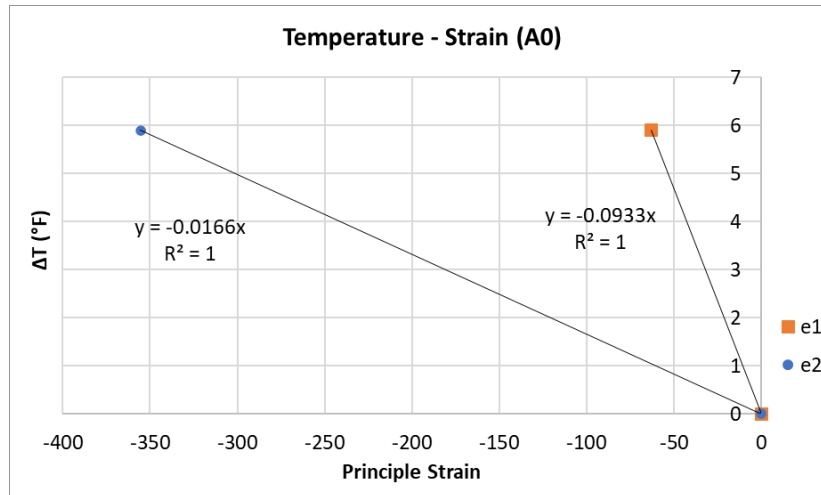


Figure 12: Test 5 (Segment A0) Web Results

6.2.4.3 Results Summary for Test 5 (Segment A0)

Segment A0 estimated RNT is found to be around 47°F-49°F, with good correlation. The web shows good longitudinal constraints, but negative strains. This could be due to one web camera being out of focus. Conclusions should not be drawn from this data due to the low number of data points.

6.2.4.4 RNT Measurements for Test 6 (Segment B0)

Segment B0 has five data sets for both top of rail and web, with temperatures between 66°F-85.6°F. Results for the top of rail can be seen below in Figure 6.11.

Segment B0				
Set	TOR (*F)	PE	k (1/mm)	St Dev
0	66	0.28	-2.7134	0.5978
1	72.3	0.98	-0.5955	0.2326
2	79.5	0.47	-1.0667	0.6639
3	83.5	0.59	2.4359	0.5299
4	84.6	0.73	5.1426	0.9285

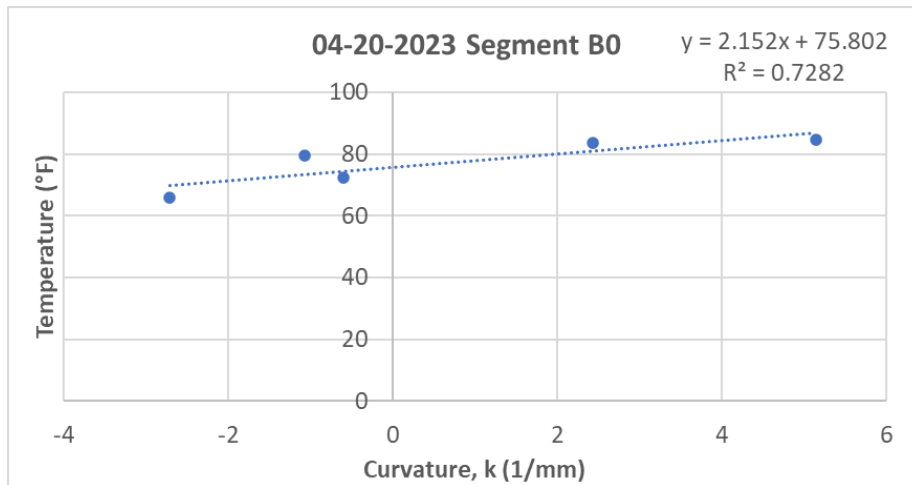


Figure 13: Test 6 (Segment B0) TOR Results

For segment B0 web analysis, set 0 and set 1 the data collected could not be processed due to low quality, so those sets were disregarded. Results for sets 2-4 can be seen below in Figure 6.12.

Segment B0			
Set	ΔT (°F)	e1	e2
2	0	0.00	0.00
3	3.1	-48.44	-436.97
4	5.4	15.42	-488.35

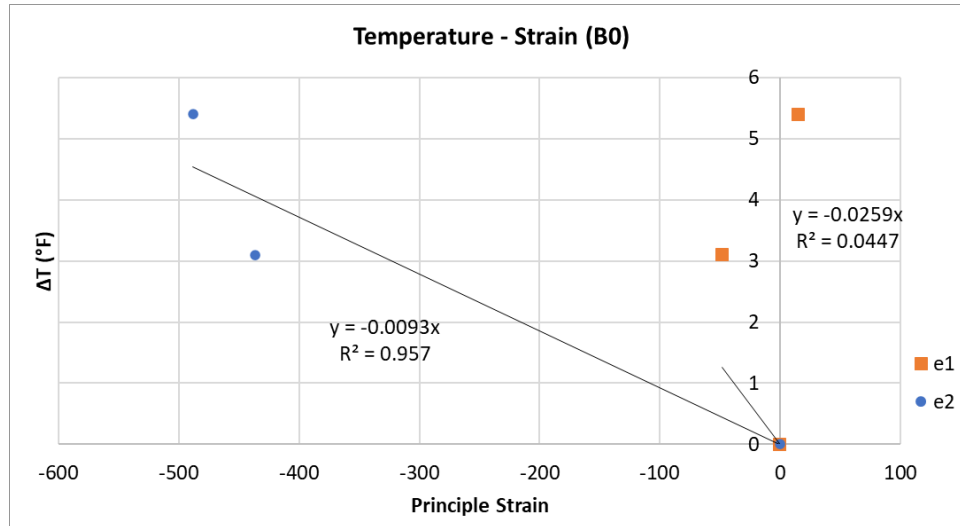


Figure 14: Test 6 (Segment B0) Web Results

6.2.4.5 Results Summary for Test 6 (Segment B0)

Segment B0 estimated RNT is approximately 76°F, with decent correlation. The web again shows good longitudinal constraints, but negative strains, similar to segment A0. This again could be due to a camera being out of focus.

6.2.4.6 Test 7 (Segment C0)

Segment C0 has only one data set, therefore could not be used for RNT estimation or strain measurements.

6.2.5 Field Tests 8, 9, and 10

6.2.5.1 Test Conditions

For the next day of testing, three more segments of rail were tested, identified as segment D0, E0, and F0. These segments were selected due to larger tie spacings, which allow

greater deformations and therefore better results. Segment D0 tie spacing (center to center) is 22.75 inches, segment E0 spacing is 22 inches, and segment F0 spacing is 25 inches. The heating method used was also a natural heating cycle. The last two data sets for all segments were taken after a train had passed over the track, and the top of rail was respeckled. Due to train passing, and therefore changing the curvature, the RNT estimation was separated as “before train” and “after train.” For all top of rail analyses, all images were processed for curvature and the average was plotted with temperature.

6.2.5.2 RNT Measurements for Test 8 (Segment D0)

A total of six data sets were collected at segment D0. Results for segment D0 TOR can be seen below in Figure 6.13.

Segment D0					
	Set	TOR (°F)	PE	Avg k (1/mm)	St Dev
Before Train	0	67.5	1.03	-1.7395	1.1846
	1	75.4	0.05	-4.0789	0.3486
	2	77	0.07	-1.8309	0.4812
	3	84.7	0.17	-3.9867	0.2959
After Train	4	92.3	0.08	-0.3509	0.3568
	5	87.9	0.1	0.7237	0.4213

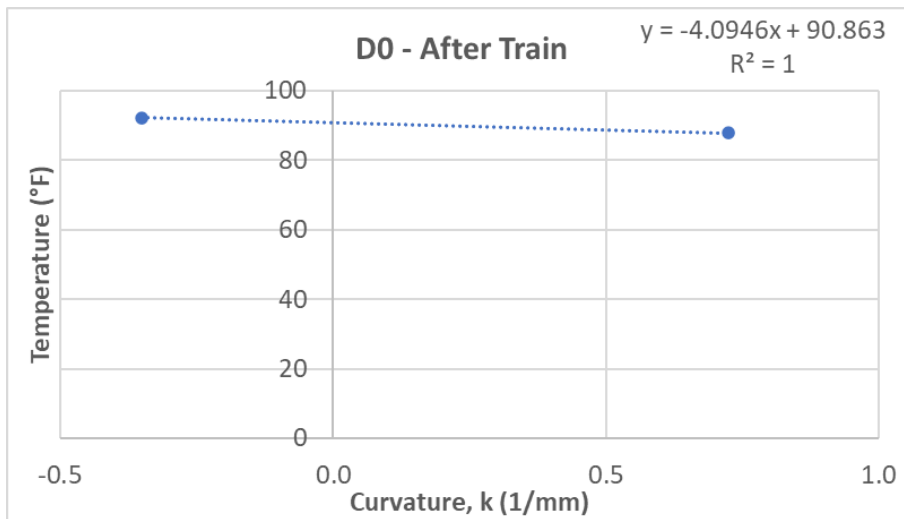
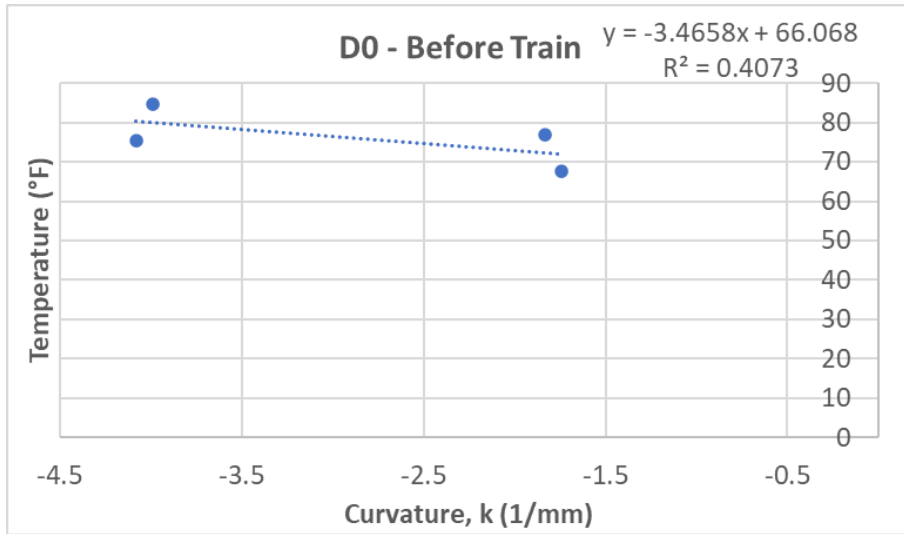


Figure 15: Test 8 (Segment D0) TOR Results

Results for segment D0 (before the train passed) web analysis can be seen below in Figure 6.14.

Segment D0			
Set	ΔT (°F)	e1	e2
0	0.0	0.00	0.00
1	8.6	598.40	-43.85
2	9.4	607.72	-19.51
3	17.6	811.22	166.80

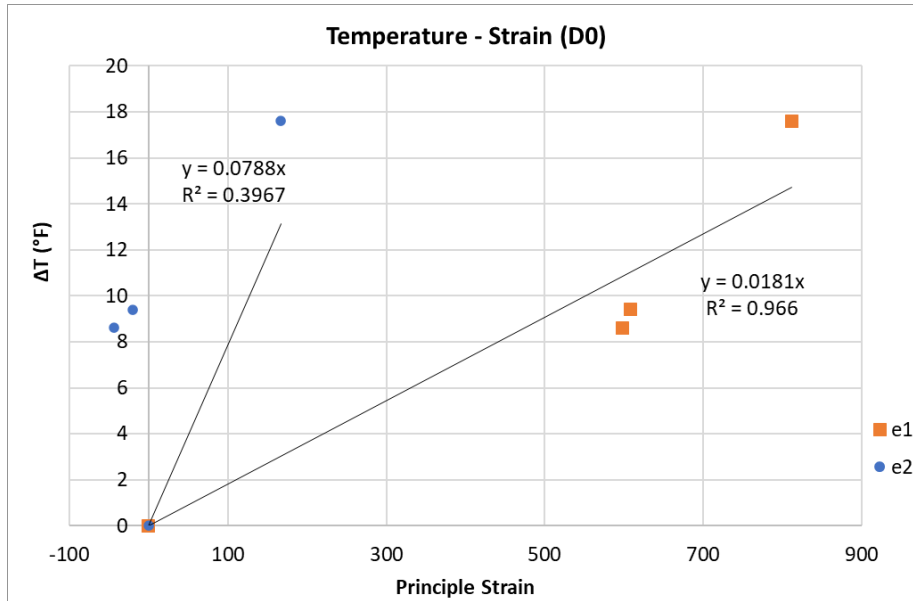


Figure 16: Test 8 (Segment D0) Web Results

6.2.5.3 Results Summary for Test 8 (Segment D0)

For the top of rail, an estimated RNT was found to be around 66°F before the train passed and increased to 90°F after the train, although the correlation is low. More data is needed to confidently estimate the RNT. The web results show high strains, which may not be reliable and could be due to errors in acquisition or processing.

6.2.5.4 RNT Measurements for Test 9 (Segment E0)

A total of six data sets were collected at segment E0. Segment E0 top of rail results can be seen below in Figure 6.15.

Segment E0					
	Set	TOR (°F)	PE	Avg K	St Dev
Before Train	0	67	0.9	4.479	0.6796
	1	72.7	0.07	3.706	0.5279
	2	78.1	0.17	3.719	0.4072
After Train	3	82.6	0.12	2.392	0.5550
	4	95	0.05	1.023	1.1282
	5	97.7	0.07	0.461	1.1964

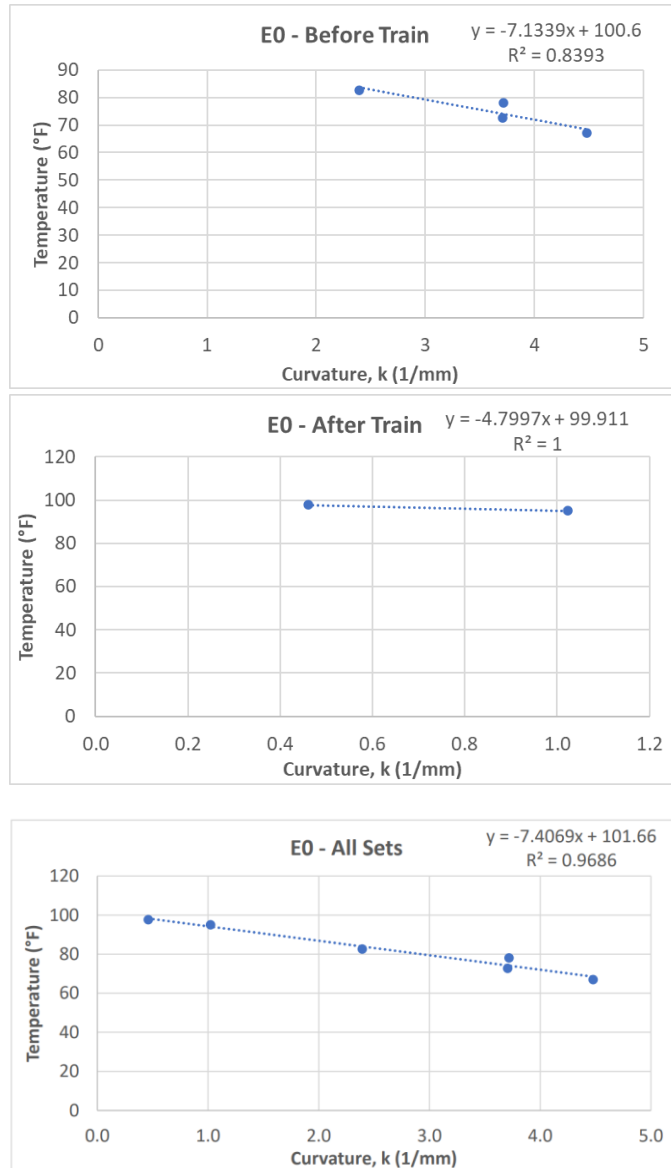


Figure 17: Test 9 (Segment E0) TOR Results

Segment E0 (before train passed) web results can be seen below in Figure 6.16.

Data set 2 was excluded due to image quality.

Segment E0			
Set	ΔT ($^{\circ}F$)	e1	e2
0	0	0.00	0.00
1	6.2	151.12	-2.57
3	15	522.28	12.02

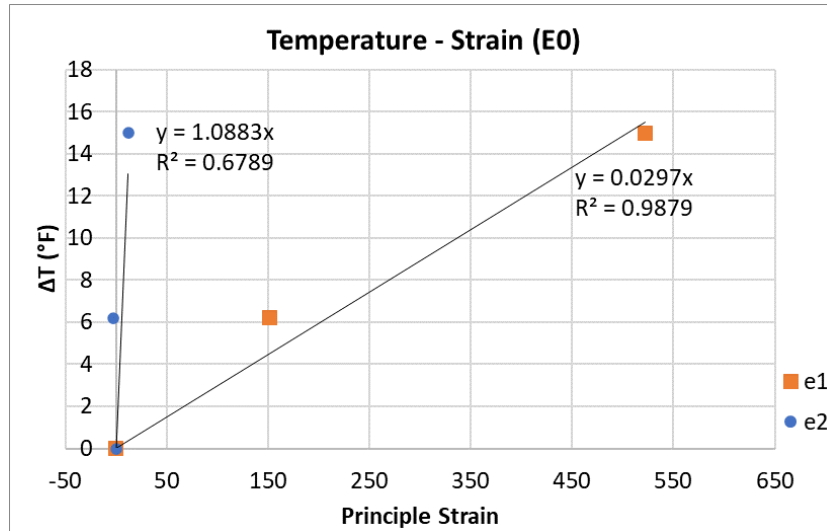


Figure 6.16: Test 9 (Segment E0) Web Results

6.2.5.5 Results Summary for Test 9 (Segment E0)

Segment E0 results show an estimated RNT of around 100 $^{\circ}F$ before and after the train passed, with decent correlation. More data points are needed for a more conclusive RNT estimate. For the web, good longitudinal constraints are observed.

6.2.5.6 RNT Measurements for Test 10 (Segment F0)

A total of four data sets were collected for segment F0. For segment F0, results can be seen below in Figure 6.17.

Segment F0					
	Set	TOR (°F)	PE	Avg K	St Dev
Before	0	68.2	0.01	0.0518	0.5015
Train	1	74.8	0.03	0.6031	0.2166
After Train	2	88	0.07	2.3904	0.8441
	3	94.6	0.03	-0.9074	0.4802

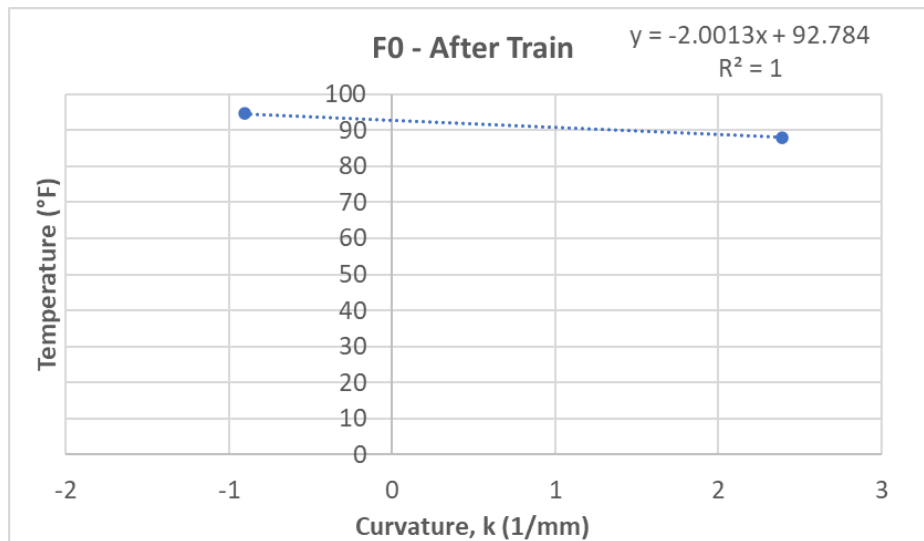
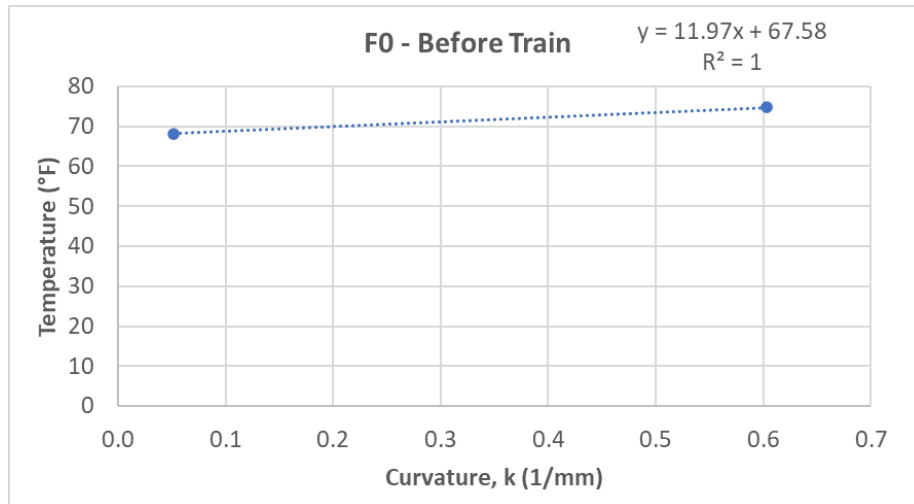


Figure 18: Test 10 (Segment F0) TOR Results

Segment F0 (before train passed) web results can be seen below in Figure 6.18.

Segment F0			
Set	ΔT (°F)	e1	e2
0	0	0.00	0.00
1	5.6	203.67	-83.58

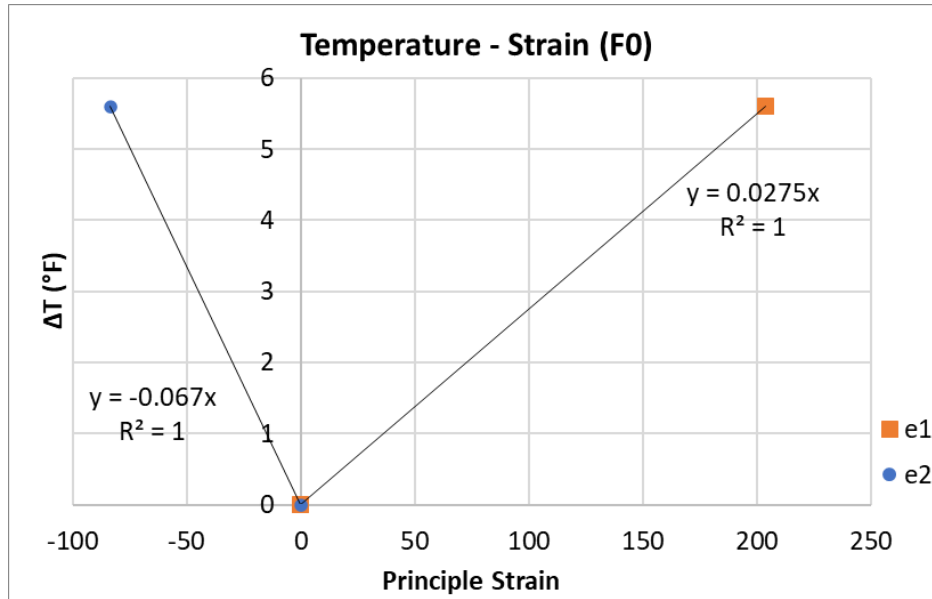


Figure 6.18: Test 10 (Segment F0) Web Results

6.2.5.7 Results Summary for Test 10 (Segment F0)

Segment F0 top of rail analysis shows an estimated RNT of approximately 68°F before the train and 93°F after the train passed, which is similar to the results for the other two segments on this day. More data sets are needed to confidently estimate the RNT.

Results for the web also show some longitudinal constraints, although again these results should not be used conclusively due to the low number of data points.

Chapter 7 Critical Discussion

This chapter discusses heating, image quality, noise, and web measurements, and gives recommendations.

7.1 Test 9 (Segment E0)

Comparing the results obtained from all field tests, test 9 provided the best results. These results provide further proof of concept, but also demonstrate the importance of obtaining proper longitudinal constraints in order to observe an accurate change in curvature with temperature. The analysis for the top of rail for this test also had overall low projection errors, which can be indicative of more reliable results. For example, the results from test 3 web strains showed the possibility of adjacent segments heating more than the segment being measured, causing opposite strains (Figure 6.6a). Test 3 also had increasing projection error scores for the top of rail analysis as well, indicating a possibly unreliable result. Test 9 shows progress in the overall system setup and areas of interest for improvement.

7.2 Acquisition Platforms

The implementation of the rail cart significantly improved the ease of measurement acquisition; however it was found through the field tests that the system is not as stable as the frame. It was observed that when processing all images from a single data set, the

image shifts slightly across the time of the images' acquisition. This slight movement could be the cause of projection errors, or changes in curvature between images across a single data set. Due to the rail cart movement between acquisitions, it might also be necessary to recalibrate the cameras more often throughout testing to verify the cameras are still in the correct position and focus. The stability of the rail cart should be improved in order to obtain higher quality results when data processing.

7.3 Heating

The two heating methods used for laboratory and field testing were induced (via industrial heat strips) and natural (via sunlight). Although an induced heating cycle reduces the overall time it takes to complete a full test, difficulties are found in terms of maintaining uniform heating. The heat strips are removed during image acquisition so that they do not affect image quality, however the constant removal and replacement may introduce other problems. When the rail is allowed to heat naturally, a more uniform heat distribution is observed and is reflected in the results showing minimal transverse strain and increasing longitudinal strain with temperature.

7.4 Image Quality

As discussed in Chapter 2.2, the quality and accuracy of results using DIC technology is directly related to the image quality. Although the most recent field tests were performed using speckle patterns that were determined to be optimal, it is just as important that the cameras are properly positioned, focused, and calibrated. During testing on April 20th, 2023, the web calibration showed good positioning and configurations (Figure 7.1). At some point, camera 1 became severely out of focus (Figure 7.2). Possibly due to the size of the calibration dots, the focus of the web cameras appeared optimal, though when

placed back in position facing the web, the focus was lost. Due to this, the results of the web analysis showed high projection errors and/or the inability for the image to be processed.

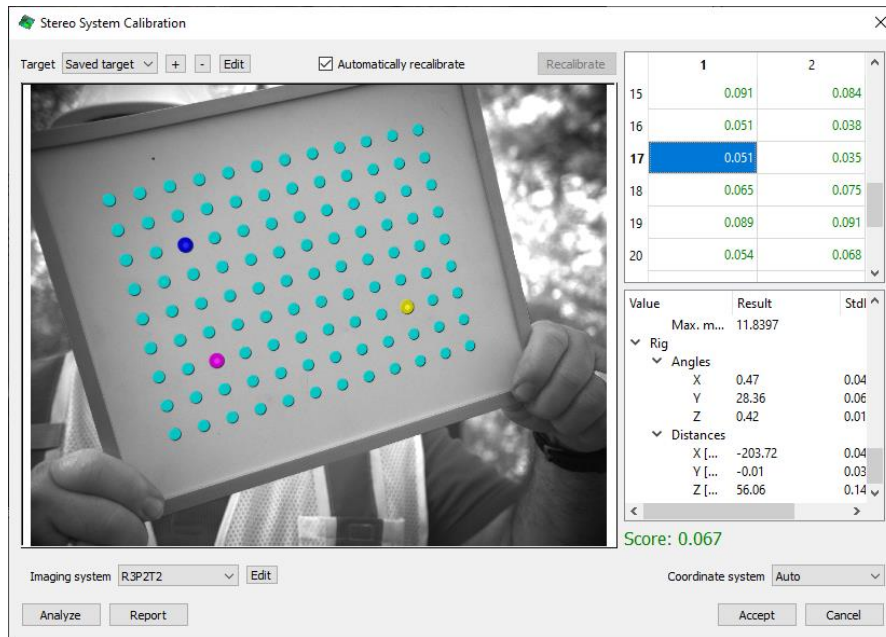


Figure 7.1: Web calibration score for field testing 04-20-2023

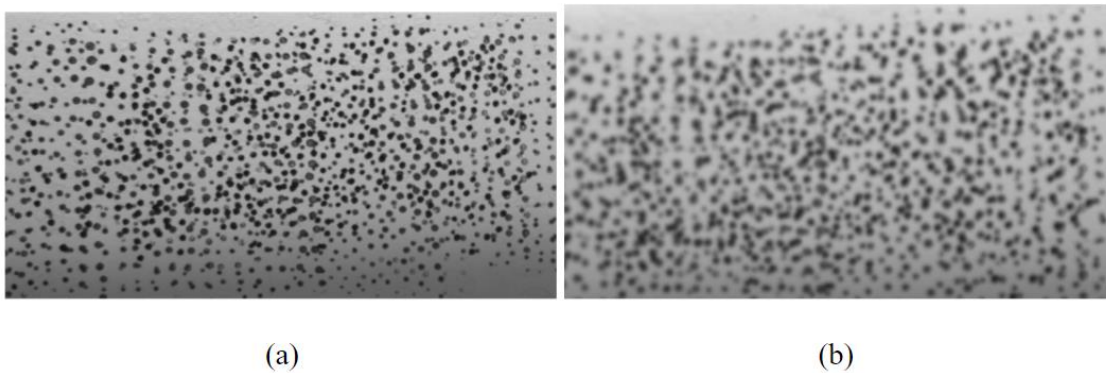


Figure 7.2: Web cameras field of view zoomed in to show quality of images of (a) camera 0 and (b) camera 1

Extra care should be taken throughout the duration of testing to ensure that all cameras maintain optimal focus and brightness settings. If focus is lost, the cameras should be adjusted and recalibrated before obtaining subsequent data sets.

7.5 Noise and Quality Control

Several methods of quality control were used during data processing to minimize the effects of noise in the results, including using the standard deviation of the data set and observing individual shape profiles for outliers. Another indication of the quality and reliability of a data set could be the projection errors observed while processing the data. Although these methods help provide some reduction in uncertainty, further investigation into other quality control methods should be done.

7.6 Web and Stress Measurements

During the field testing performed in June 2022, the addition of extra rail clips was tested to see if it would provide better longitudinal constraints on the rail. Results showed an improvement in web results compared to previous tests, confirming this idea. Although results from web analysis are acceptable, more work should be done regarding the speckling of the web. The quality of the web speckle directly relates to the quality and reliability of the web processing, and current techniques used to speckle the web should be improved.

Chapter 8 Conclusions

This chapter presents the final conclusions for this thesis.

8.1 Conclusions

This thesis presents the continuation of work that began with Knopf's proposed system and methodology for estimating RNT and longitudinal stress in CWR, followed by Chao's work developing the first-generation prototype of a non-contacting, reference-free measurement system. The continuation of laboratory and field testing provides data to further develop and optimize the full-scale measurement system. More studies have been presented investigating other variables in the system and the effects on results. Work was done to verify the accuracy and possible radial distortion of the StereoDIC camera systems using a milled granite slab with a known tolerance, as well as determining optimal camera positions, and optimal speckle patterns. The effects of shadows on the specimen during data acquisition were also resolved by using blue filters on the camera lenses in conjunction with blue lights and sunlight shades. Investigation into acquisition and analysis methods show promising results regarding independent shape measurements as opposed to correlating data across temperatures. This is a significant improvement to the overall system as now it can be moved between acquisitions. Previously, any rigid body motion of the system would present issues when processing the data by correlating across temperatures. This also now allows for more than one segment of rail to be tested

at a time, which gives confidence in the data results. Work was also done to condense the equipment to a single rail cart, to allow easier transport and movement between rail segments to be tested.

Upon completion of this work, the following conclusions can be made:

- Better results are obtained when the rail has strong longitudinal constraints.
When selecting a rail segment to test in the field, ideally the segment should have additional rail clips installed to the adjacent ties.
- The RNT of a rail segment can be determined by processing the shape at each temperature, rather than correlating across temperatures.
- Maintaining good calibration throughout the duration of a test is very important.
Calibration should be performed at the end of testing to verify the system parameters remained the same.

8.2 Future Work

This thesis presents the third phase of a multi-phase project, therefore more work is to be done. Recommendations for future work include:

- Investigation into statistical methods to filter the data outliers when processing shape measurements.
- Improvement on speckle patterns and web pattern application.
- Investigation of possible sources of high projection errors in field data.

References

- A. A. Rashid, R. I. (2020). Determination of opening stresses for railway steel under low cycling fatigue using digital image correlation. *Theoretical and Applied Fracture Mechanics*, 108.
- A. Abdulqader, D. C. (2020). Benefits of digital image correlation in uniaxial compression tests. *Results in Engineering*, 6.
- Abdulqader, A. H. (2017). *Product Qualification and Performance Assessment of HSRM Prestressed Concrete Railroad Ties through Laboratory Testing*. Master of Science Thesis, University of South Carolina, Department of Civil and Environmental Engineering.
- Association of American Railroads. (2022, October). Freight Rail's Economic Impact. *Association of American Railroads*.
- C. A. Murray, A. W. (2015). Measurement of vertical and longitudinal rail displacements using digital image correlation. *Canadian Geotechnical Journal*, 52(2), 141-155.
- Chao, E. Y.-H. (2022). *Development of a First-Generation Prototype Laboratory System for Rail Neutral Temperature Measurements*. Master of Science Thesis, University of South Carolina, Department of Civil and Environmental Engineering, Columbia, SC.

Enshaeian, A., & Rizzo, P. (2021). Stability of continuous welded rails: A state-of-the-art review of structural modeling and nondestructive evaluation. *Proceedings of the Institution of Mechanical Engineers, Part F: Journal of Rail and Rapid Transit*, 235(10), 1291-1311. doi:10.1177/0954409720986667

Knopf, K. (2019). *A Non-Contacting System for Rail Neutral Temperature and Stress Measurements*. Master of Science Thesis, University of South Carolina, Department of Civil and Environmental Engineering, Columbia, SC.

Knopf, K., Rizos, D. C., Qian, Y., & Sutton, M. (2021). A non-contacting system for rail neutral temperature and stress measurements: Concept development. *Structural Health Monitoring*, 20(1), 84-100. doi:10.1177/1475921720923116

Knopf, K., Rizos, D. C., Qian, Y., & Sutton, M. (2022). On the Validation and Implementation of a Vision-Based Concept for Rail Neutral Temperature and Stress Measurements. *Proceedings of AREMA 2020 Virtual Conference*.

Knopf, K., Rizos, D., Qian, Y., & Sutton, M. (2020). A Stereovision System for Rail Neutral Temperature Measurements and Effects of the Heating Method. *Proceedings of the 2020 Joint Rail Conference, JRC2020-8119*. St. Louis, MO.

M. A. Sutton, F. M. (2017). Recent Progress in Digital Image Correlation: Background and Developments since the 2013 W M Murray Lecture. *Experimental Mechanics*, 57, p. 30.

M. A. Sutton, J. H.-J. (2008). The effect of out-of-plane motion on 2D and 3D digital image correlation measurements. *Optics and Lasers in Engineering*, 46(10), 746-757.

- M. A. Sutton, J. J. (2009). *Image Correlation for Shape, Motion, and Deformation Measurements*. Springer.
- M. A. Sutton, W. J. (1983). Determination of displacements using an improved digital image correlation method. *Image Vis Comput*, 1(3), 1333-1339.
- Reu, P. (2014). The Art and Application of DIC; Speckle Size Measurement. *Experimental Techniques*, 38, 1-2.
- Reu, P. (2014). The Art and Application of DIC; Speckles and their relationship to the digital camera. *Experimental Techniques*, 38, 1-2.
- Reu, P. (2015). The Art and Application of DIC; All about speckles. *Experimental Techniques*, 39, 1-2.
- Reu, P. (2015). The Art and Application of DIC; All About Speckles: Contrast. *Experimental Techniques*, 39, 1-2.
- Reu, P. (2015). The Art and Application of DIC; All About Speckles: Edge Sharpness. *Experimental Techniques*, 39, 1-2.
- Reu, P. (2015). The Art and Application of DIC; All about speckles: Speckle Density. *Experimental Techniques*, 39, 1-2.
- Reu, P. (2015). The Art and Application of DIC; Points on Paint. *Experimental Techniques*, 39, 1-2.
- Rizos, D. C. (2018). *US Patent No. PCT/US2019/026267*.
- Rizos, D. C., Chao, E., Stinson, B., Penna, C., Sutton, M., & Wilson, R. (2022). A Non-Destructive, Reference-Free Procedure for RNT and Longitudinal Stress

- Measurements: Field Implementation and Validation. *Proceedings of AREMA 2022 Annual Conference and Exposition*. Denver, CO.
- S. Yaofeng, J. H. (2007). Study of optimal subset size in digital image correlation of speckle pattern images. *Optics and Lasers in Engineering*, 45, 967-974.
- Standardization, G. P. (2018). A Good Practices Guide for Digital Image Correlation. *International Digital Image Correlation Society*, 1-110.
- Stinson, B., Penna, C., Gedney, B., Rizos, D. C., & Sutton, M. (2023). Field Implementation of Stereo Vision System for RNT and Longitudinal Stress Measurements in CWR Track. *Proceedings of the ASME 2023 Joint Rail Conference*. Baltimore, MD.
- W. H. Peters III, W. F. (1983). Application of digital image correlation methods to rigid body mechanics. *Optics and Lasers in Engineering*, 22(6), 738-743.
- Wyatt, T. (2023). *Speckle Development and Application in UAV-Based Digital Image Correlation for Transportation Infrastructure Monitoring and Assessment*. Master of Science Thesis, University of South Carolina, Department of Civil and Environmental Engineering, Columbia, SC.
- Yun, H.-B., Lee, K.-C., Park, Y.-J., & Jung, D.-K. (2019). Rail neutral temperature monitoring using non-contact photoluminescence piezospectroscopy: A field study at high-speed rail track. *Construction and Building Materials*, 204, 357-370.